

# A physics-preserving pure streamfunction formulation and high-order compact solver with high-resolution for three-dimensional steady incompressible flows

Bo Peng (彭博), Xiaohu Guo, Yingqing Zu (祖迎庆),  
and Zhenfu Tian

## Published version information

**Citation:** B Peng et al. A physics-preserving pure streamfunction formulation and high-order compact solver with high-resolution for three-dimensional steady incompressible flows. *Phys Fluids* 35, no. 4 (2023): 043104

**DOI:** [10.1063/5.0140054](https://doi.org/10.1063/5.0140054)

This article may be downloaded for personal use only. Any other use requires prior permission of the author and AIP Publishing. This article appeared as cited above. This version is made available in accordance with publisher policies. Please cite only the published version using the reference above. This is the citation assigned by the publisher at the time of issuing the APV. Please check the publisher's website for any updates.

RESEARCH ARTICLE | APRIL 07 2023

## A physics-preserving pure streamfunction formulation and high-order compact solver with high-resolution for three-dimensional steady incompressible flows

Peng Bo (彭博); Xiaohu Guo; Zu Yingqing (祖迎庆); ... et. al



*Physics of Fluids* 35, 043104 (2023)

<https://doi.org/10.1063/5.0140054>



CrossMark

### Articles You May Be Interested In

The concept of streamfunctions in the Wien effect on a weak electrolyte

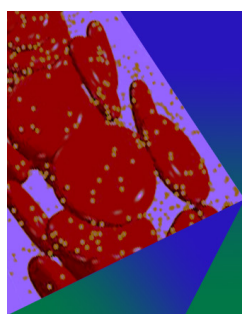
*J. Math. Phys.* (December 1987)

Vortex drift. II: The flow potential surrounding a drifting vortical region

*Physics of Fluids A: Fluid Dynamics* (June 1993)

Dynamical forecast experiments with a baroclinic quasigeostrophic open ocean model

*AIP Conference Proceedings* (January 1984)



## Physics of Fluids

### Special Topic: Flow and Forensics

Submit Today!



# A physics-preserving pure streamfunction formulation and high-order compact solver with high-resolution for three-dimensional steady incompressible flows

Cite as: Phys. Fluids **35**, 043104 (2023); doi: 10.1063/5.0140054

Submitted: 27 December 2022 · Accepted: 8 March 2023 ·

Published Online: 7 April 2023



View Online



Export Citation



CrossMark

Bo Peng (彭博),<sup>1</sup> Xiaohu Guo,<sup>2</sup> Yingqing Zu (祖迎庆),<sup>1</sup> and Zhenfu Tian (田振夫)<sup>1,3,a)</sup>

## AFFILIATIONS

<sup>1</sup>Department of Aeronautics and Astronautics, Fudan University, Shanghai 200433, People's Republic of China

<sup>2</sup>Hartree Centre, Science and Technology Facilities Council, Daresbury Laboratory, Sci-Tech Daresbury, Keckwick Lane, Daresbury, Warrington, Cheshire WA4 4AD, United Kingdom

<sup>3</sup>Research Institute of Intelligent Complex Systems, Fudan University, Shanghai 200433, People's Republic of China

a) Author to whom correspondence should be addressed: [zftian@fudan.edu.cn](mailto:zftian@fudan.edu.cn) and [z.f.tian@126.com](mailto:z.f.tian@126.com)

## ABSTRACT

In this paper, a pure streamfunction high-order compact (HOC) difference solver is proposed for three-dimensional (3D) steady incompressible flows. A physics-preserving pure streamfunction formulation is first introduced for the steady 3D incompressible Navier–Stokes (NS) equations without in-flow and out-flow boundary conditions, where the divergence of streamfunction  $\nabla \cdot \psi$  is maintained in the convective and the vortex-stretching terms together in the nonlinear term of equations to reduce the physics-informed loss. Moreover, taking the streamfunction-vector components and their first-order partial derivatives as unknown variables, some fourth-order compact schemes are suggested for the partial derivatives that appear in the streamfunction formulation, and a high-resolution HOC scheme is introduced for approximating the pure third-order partial derivatives in the convective term. Meanwhile, a new HOC scheme is proposed for the first-type boundary conditions of the streamfunction. Finally, a fourth-order compact difference scheme and its algorithm are established for the 3D steady incompressible NS equations in the streamfunction form, subject to no in-flow and out-flow boundary conditions. Several numerical examples are carried out to validate and prove the accuracy, convergence, and efficiency of the proposed new method. Numerical results reveal that the proposed method not only can achieve fourth-order accuracy but also has excellent convergence, high-resolution, and low computational cost at higher Reynolds number.

Published under an exclusive license by AIP Publishing. <https://doi.org/10.1063/5.0140054>

## I. INTRODUCTION

Numerical solution of the incompressible Navier–Stokes (NS) equations has remained an attractive research theme in the past decades due to its significance in a wide range of physics and engineering problems.<sup>1–17</sup> According to the use of mathematical formulations, the NS equations may be divided into three major categories, namely the primitive-variable formulation, the vorticity formulation, and the pure streamfunction formulation. The main advantage of utilizing the primitive flow variables (velocity, pressure) approach should be that a better insight into the physical conservation laws and their boundary conditions can be provided, and 2D and 3D flows may be conducted equally well with similar algorithms. The biggest difficulty for the numerical solution of the primitive variable formulation is that the

pressure is coupled implicitly with the divergence-free constraint on the velocity field in the continuity equation for incompressible flow owing to the lack of a physically meaningful pressure equation. The vorticity-streamfunction/vorticity-velocity formulation offers an alternative to the primitive-variable formulations of incompressible NS equations.<sup>16,18</sup> Its biggest advantage is eliminating problems related to the velocity–pressure decoupling because the pressure gradient terms do not arise in the vorticity transport equation, while the continuity equation (the mass conservation) is automatically satisfied in the process of the derivation of the vorticity equation. Another advantage is the resulting system of equations in the closed form, which makes it amenable to fast numerical integration with appropriate iterative or direct solvers.<sup>16</sup> These two advantages make the vorticity-streamfunction formulation very

attractive for solving high Reynolds number planar or axisymmetric NS equations accurately. However, the use of the vorticity formulations is still affected owing to a few drawbacks. The main drawback is the necessity to use approximate and iterative vorticity boundary conditions along solid walls because of the absence of the physical boundary condition for the vorticity variables. Thus, the construction of numerical boundary conditions has to be carried out for the vorticity variables. The utilization of the pure streamfunction formulation has two remarkable advantages compared with the NS equations in terms of primitive variables. The continuity equation is the automatic satisfaction, and the pressure is eliminated from the governing equations. The velocity divergence-free constraint is the primary challenge in various primitive variable approaches.<sup>19</sup> Compared with various vorticity formulations, the main advantage of the use of the pure streamfunction formulation is that the boundary conditions are generally known for 2D problems; while, for 3D problems, the boundary conditions including the enforced one to ensure the vector potential's existence and uniqueness mathematically can always be provided for the streamfunction, and fewer pure numerical boundary conditions are required to be established for the derivatives of streamfunction.<sup>5</sup>

For 2D flow problems, the advantages of the pure streamfunction formulation have been well exploited to achieve numerical advantages.<sup>3,20–28</sup> However, to best of the authors' knowledge, there are only a few numerical works found for the 3D pure streamfunction (vector-potential) formulation in recent years<sup>2,5,29–31</sup> due to the great challenge of how to introduce boundary condition for the streamfunction  $\psi$  to eliminate the ambiguity of  $\psi$  (Refs. 2 and 6) and approximate it accurately.<sup>5</sup> In fact, the primary purpose of introducing the boundary condition is to enforce  $\nabla \cdot \psi = 0$ , namely, the divergence-free constraint of streamfunction, so that the solution for  $\psi$  exists and is unique mathematically.<sup>2,5,6</sup> Fishelov *et al.*<sup>2</sup> utilized  $\Delta(\nabla \cdot \psi) = 0$  on the boundaries that is termed as "Second-type boundary condition" (BC2) to develop the 3D pure streamfunction formulation with a set of boundary conditions with non-penetration and proposed a fourth-order compact scheme, in which the grid values of the streamfunction and its first derivatives were regarded as the unknown variables. The developed scheme was only validated by a simple numerical example with an exact solution because the corresponding schemes on the boundary conditions were not established. Moreover, it should be noted that the pure streamfunction formulation proposed in Ref. 5 actually maintains  $\nabla \cdot \psi$  in the vortex-stretching term in the nonlinear term. This modified formulation guaranteed that the convergent numerical solutions can be obtained for all test problems including more strong singularity problems, such as the lid-driven cavity flow by two perpendicular walls<sup>32,33</sup> and a diagonally lid-driven cubic cavity flow that was first investigated by Povitsky,<sup>34</sup> which was studied numerically<sup>32,33,35</sup> and has become a benchmark case for developing numerical methods.<sup>5,36,37</sup> Unfortunately, it is found that the convergent numerical solutions obtained in Ref. 5 for a diagonally lid-driven cubic cavity flow is not accurate and stable (see Sec. V for details). The reason for this should be that the  $\nabla \cdot \psi$  is not fully preserved in the nonlinear terms, and the boundary condition  $\vec{n} \cdot \nabla(\nabla \cdot \psi) = 0$  is not fully translated into tangent directions, which lead to underutilization of the physical information of boundary conditions. Actually, the discrete  $\nabla \cdot \psi$  cannot be considered strictly zero, because the discretized boundary condition  $\vec{n} \cdot \nabla(\nabla \cdot \psi) = 0$  also has error. Therefore,  $\nabla \cdot \psi$  should be maintained in the nonlinear terms involving the convective and the

vortex-stretching terms, which may be interpreted as the physics-informed  $\nabla \cdot \psi$  preserving in the pure streamfunction formulation. In addition, the boundary condition  $\vec{n} \cdot \nabla(\nabla \cdot \psi) = 0$  should be fully translated into tangent directions. The discretization of boundary conditions in tangential direction can make better use of the physical information on the boundaries than that of boundary conditions in the normal direction, which helps to improve the accuracy and efficiency of numerical methods.

High-order difference methods have received considerable attention in the past three decades because of their potential in delivering higher accuracy with lower computational cost than low-order accuracy methods.<sup>2,4,5,20,23,38–40</sup> In addition, high-order numerical methods are fully recognized in very deep and detailed studies of complex physical phenomena. A review of the current status of the high-order methods along with their applications was presented by Wang *et al.*<sup>39</sup> High-order difference methods can be classified as wide (explicit) and compact (implicit) or Padé type. Explicit high-order schemes calculate or discrete the derivatives directly at each grid using a wider computational stencil, while compact schemes evaluate the derivatives along a grid line using smaller stencils and solving a linear system. Previous experiences show that compact schemes are more accurate than the corresponding explicit scheme of the same order. The readers are referred to a very recent paper<sup>40</sup> for details and references therein. For the discretization of the pure streamfunction formulation being a fourth-order nonlinear partial differential equation, utilizing the traditional explicit central difference method has great disadvantages. Actually, to obtain the classical second-order and fourth-order accuracy difference approximation for the pure third- and fourth-order derivatives, 5-point and 7-point difference stencils are required, respectively; while for approximating the mixed third- and fourth-order derivatives, in 2D case, 9-point and 27-point difference stencils, and in 3D case, 25-point and 125-point difference stencils are demanded, respectively. Obviously, this central difference approximation using multipoint wide difference stencils has to be amended at grid points near the boundaries and is sure to bring about difficulties for the solution of the resulting linear systems. Therefore, the development of high-order of accuracy compact difference method using smaller difference stencil should be an effective way for solving 3D pure streamfunction formulation.

The objective of this paper is to develop a physics-preserving pure streamfunction formulation-based high-resolution high-order compact (HOC) difference method for solving 3D incompressible NS equations with no in-flow and out-flow boundary conditions. The main characteristic of the physics-preserving pure streamfunction formulation is that the divergence-free constraint of streamfunction-vector is not imposed in the nonlinear term of the pure streamfunction formulation, namely  $\nabla \cdot \psi$  maintains in the convective and the vortex-stretching terms to reduce the physics-informed loss, which means the developed HOC scheme maintains a particular discrete form of the streamfunction-vector divergence around the machine round-off error as long as the boundary conditions are compatible with the constraints. In the present work, the streamfunction-vector components and their first-order partial derivatives are regarded as the unknown variables in the establishment of the finite difference method. In addition, a high-resolution HOC scheme is suggested for approximating the third-order partial derivatives in the convective terms, and a new high-order numerical boundary scheme is proposed



for BC1. Finally, a comprehensive evaluation on the validity of the high-resolution physics-preserving pure streamfunction HOC difference solver is conducted by using numerical examples such as an analytic solution and the lid-driven cubic cavity flow and the diagonally lid-driven cubic cavity flow problems. Compared to Ref. 5, there are the following advantages/novelties of this study. First of all, the divergence of streamfunction  $\nabla \cdot \psi$  is preserved in the convective and the vortex-stretching terms, and this streamfunction formulation makes more physical sense. Second, some extra errors caused by numerical boundary schemes constructed not being physically given for the second derivatives are avoided, because the second derivatives are not taken as the unknown variables. Once more, a new high-order numerical boundary scheme is proposed for BC1 based on the boundary condition  $\vec{n} \cdot \nabla(\nabla \cdot \psi) = 0$  translated into tangent directions. Finally, HOC schemes developed for approximating the third-order partial derivatives have better dispersion property and higher resolution. These would be also reflected by numerical examples in Sec. V.

This paper is structured as follows. In Sec. II, the governing equations of the streamfunction formulation in 3D incompressible viscous flows are reviewed, and the first-type “no in-flow and out-flow” boundary conditions for the streamfunction are also given by Proposition 1. In Sec. III, based on some basic discrete approximations for the first-order partial derivative and boundary closure conditions, the high-order approximations for second-, third-, and fourth-order partial derivatives are derived. The whole numerical method is established for the physics-preserving pure streamfunction formulation in Sec. IV. Numerical experiments for three test problems are performed to validate the accuracy, efficiency, and robustness of the derived HOC difference scheme in Sec. V. Conclusions are included in Sec. VI.

## II. GOVERNING EQUATIONS AND BOUNDARY CONDITIONS

### A. Governing equations

For 3D steady incompressible viscous flows in the cases of no in-flow and out-flow on the boundaries, the dimensionless governing equations in vorticity-velocity form is

$$\begin{aligned}\nabla \times (\omega \times \mathbf{u}) &= \frac{1}{Re} \Delta \omega, \quad \text{in } \Omega, \\ \omega &= \nabla \times \mathbf{u}, \quad \nabla \cdot \mathbf{u} = 0, \quad \text{in } \Omega, \\ \mathbf{u} &= \mathbf{u}_b, \quad \mathbf{n} \cdot \mathbf{u}_b = 0 \quad \text{on } \partial\Omega,\end{aligned}\quad (1)$$

in which  $\Omega$  is a bounded domain in  $R^3$ ,  $\omega$  is the vorticity vector,  $\mathbf{u} = (u, v, w)^T$  is the velocity vector,  $\mathbf{n}$  indicates the outward unit vector normal at the boundary, and  $Re$  is the Reynolds number being defined as the ratio of inertial force to viscous force within the fluid given by  $Re = \frac{UL}{\nu} \left( = \frac{\rho UL}{\mu} \right)$  with a characteristic length  $L$  and a characteristic velocity  $U$ , where  $\rho$ ,  $\nu$ , and  $\mu$  are the fluid density (assumed to be constant), the kinematic viscosity, and the fluid viscosity, respectively. Note that the boundary condition  $\mathbf{n} \cdot \mathbf{u}_b = 0$  was called as no in-flow and out-flow case in Ref. 6.

Since  $\nabla \cdot \mathbf{u} = 0$ , a vector potential, called as streamfunction vector ( $\psi = (\psi_1, \psi_2, \psi_3)^T$ ) is introduced by

$$\nabla \times \psi = \mathbf{u}. \quad (2)$$

Unlike streamfunction in 2D, however, Eq. (2) does not define  $\psi$  uniquely. Since, if  $\psi$  satisfies Eq. (2), it is also true that  $\psi + \nabla \xi$

satisfies Eq. (2) for any smooth scalar function  $\xi$ , which is known as the gauge freedom. To fix the gauge, the extra restrictions are needed at the boundaries to eliminate the ambiguity of  $\psi$  (Refs. 2 and 5), which enforces  $\nabla \cdot \psi = 0$  in  $\Omega$ . See also Ref. 6.

**Proposition 1.** Equation (1) with Eq. (2) is equivalent to

$$\begin{aligned}\nabla \times ([\nabla \times (\nabla \times \psi)] \times \mathbf{u}) &= -\nu \Delta^2 \psi, \quad \text{in } \Omega, \\ \mathbf{n} \times \psi|_{\partial\Omega} &= 0, \\ \mathbf{n} \times (\nabla \times \psi)|_{\partial\Omega} &= \mathbf{n} \times \mathbf{u}_b, \\ \frac{\partial(\psi \cdot \mathbf{n})}{\partial n} \Big|_{\partial\Omega} &= 0, \quad \frac{\partial(\nabla \cdot \psi)}{\partial n} \Big|_{\partial\Omega} = 0,\end{aligned}\quad (3)$$

where  $\mathbf{u} = \nabla \times \psi$  and  $\nu = \frac{1}{Re}$ .

Proposition 1 can be proved by referring to Ref. 6.

It is found from Eq. (3) that it could be difficult to calculate or discretize the nonlinear term  $\nabla \times ([\nabla \times (\nabla \times \psi)] \times \mathbf{u})$  in the formulation directly. Thus, by virtue of vector identity, the governing equation in Proposition 1 is equivalent to

$$(\mathbf{u} \cdot \nabla)[\nabla(\nabla \cdot \psi) - \Delta \psi] = ([\nabla(\nabla \cdot \psi) - \Delta \psi] \cdot \nabla) \mathbf{u} - \nu \Delta^2 \psi, \quad \text{in } \Omega, \quad (4)$$

where  $(\mathbf{u} \cdot \nabla)[\nabla(\nabla \cdot \psi) - \Delta \psi] = (\mathbf{u} \cdot \nabla)\omega$ , which accounts for the changes in vorticity due to the motion of the fluid particle, is termed as the convection term; while  $([\nabla(\nabla \cdot \psi) - \Delta \psi] \cdot \nabla)\mathbf{u} = (\omega \cdot \nabla)\mathbf{u}$ , which represents the effects of vortex stretching and tilting, is termed as the vortex stretching term.

Noting that the fact  $\mathbf{u} = \nabla \times \psi$  and using  $\nabla \cdot \psi = 0$  in  $\Omega$ , the governing equation (4) can be reduced to

$$((\nabla \times \psi) \cdot \nabla) \Delta \psi = (\Delta \psi \cdot \nabla)(\nabla \times \psi) + \nu \Delta^2 \psi, \quad \text{in } \Omega. \quad (5)$$

This formulation matching the BC2 was proposed by Fishelov *et al.*<sup>2</sup> It matches the BC1 in Proposition 1, which was also introduced,<sup>5</sup> and it is regarded as the simplified streamfunction formulation.

However, as seen from Ref. 5, when a flow problem with a stronger singularity, i.e., a diagonally lid-driven cavity flow, is calculated numerically, the simplified streamfunction formulation-based HOC scheme proposed cannot achieve convergent numerical results. As a result, the following modified streamfunction formulation was suggested in Ref. 5:

$$\begin{aligned}((\nabla \times \psi) \cdot \nabla) \Delta \psi \\ = ([\Delta \psi - \nabla(\nabla \cdot \psi)] \cdot \nabla)(\nabla \times \psi) + \nu \Delta^2 \psi, \quad \text{in } \Omega.\end{aligned}\quad (6)$$

The modified streamfunction formulation-based HOC method established in Ref. 5 obtained convergent results for the flow problem with a stronger singularity. Yet, why is the convergent solution obtained using the modified streamfunction formulation-based HOC method, and how accurate is it? There is no further discussion regarding this in Ref. 5.

In fact, the boundary condition  $\vec{n} \cdot \nabla(\nabla \cdot \psi) = 0$  is introduced to ensure that  $\nabla \cdot \psi = 0$ , so that the solution of  $\psi$  exists and is unique. However, the discretized  $\vec{n} \cdot \nabla(\nabla \cdot \psi) = 0$  is not exactly satisfied, so it is impossible to strictly guarantee  $\nabla \cdot \psi = 0$  everywhere in  $\Omega$ . On the other hand, keeping  $\nabla \cdot \psi$  containing the actual physical information in the model formulation (4) can maintain the conservation law of physics to the greatest extent. Therefore, the use of the formulation (4)

should be more accurate, reliable, and efficient both numerically and physically. This would be verified through numerical results in Sec. V.

In this work, the formulation (4) would be called as the physics-preserving streamfunction formulation because  $\nabla \cdot \psi$  is fully preserved in the nonlinear terms, i.e., the convection term and the vortex-stretching term. Moreover, a fourth-order compact difference method based on Proposition 1 is established for the physics-preserving streamfunction formulation (4), where a newly proposed numerical boundary scheme is included as well.

## B. Boundary conditions

Notice from Proposition 1 that there are six independent scalar boundary conditions given for  $\psi$ . To describe the boundary conditions intuitively, without loss of generality, let us consider a problem in the cubic cavity of  $[0, 1]^3$ . For simplicity, taking the face  $z = 1$  as an example, a brief description and treatment for the boundary conditions in Proposition 1 is listed as follows.

The boundary conditions at the face  $z = 1$  in Proposition 1, without any processing, can be written as

$$\begin{aligned} \psi_1 = \psi_2 = 0, \\ \frac{\partial \psi_1}{\partial z} = \frac{\partial \psi_3}{\partial x} + v_b, \quad \frac{\partial \psi_2}{\partial z} = \frac{\partial \psi_3}{\partial y} - u_b, \quad \frac{\partial \psi_3}{\partial z} = 0, \\ \frac{\partial}{\partial z} \left( \frac{\partial \psi_1}{\partial x} + \frac{\partial \psi_2}{\partial y} + \frac{\partial \psi_3}{\partial z} \right) = 0. \end{aligned} \quad (7)$$

In order to obtain  $\psi_3$  at the face  $z = 1$ , we need to deal with the last boundary condition in Eq. (7), which can be rewritten as

$$\begin{aligned} \frac{\partial^2 \psi_3}{\partial z^2} &= -\frac{\partial}{\partial x} \left( \frac{\partial \psi_1}{\partial z} \right) - \frac{\partial}{\partial y} \left( \frac{\partial \psi_2}{\partial z} \right) \\ &= -\frac{\partial}{\partial x} \left( \frac{\partial \psi_3}{\partial x} + v_b \right) - \frac{\partial}{\partial y} \left( \frac{\partial \psi_3}{\partial y} - u_b \right), \end{aligned} \quad (8)$$

which is equivalent to

$$\frac{\partial^2 \psi_3}{\partial z^2} = -\frac{\partial^2 \psi_3}{\partial x^2} - \frac{\partial^2 \psi_3}{\partial y^2} - \frac{\partial v_b}{\partial x} + \frac{\partial u_b}{\partial y}. \quad (9)$$

It can easily be noticed from the above-mentioned equations that the boundary condition for  $\psi_3$  is not given directly. It need to be decided by its first partial derivative with respect to  $z$  and other boundary conditions, such as Eq. (9).

**Remark 2.1.** According to Ref. 5, for the condition  $\frac{\partial(\nabla \cdot \psi)}{\partial n} = 0$  at the boundary  $z = 1$ ,

$$\frac{\partial^2 \psi_3}{\partial z^2} = -\frac{\partial}{\partial z} \left( \frac{\partial \psi_1}{\partial x} + \frac{\partial \psi_2}{\partial y} \right) = -\frac{\partial^2 \psi_1}{\partial z \partial x} - \frac{\partial^2 \psi_2}{\partial z \partial y} \quad (10)$$

was derived. Compared with the right-hand side of Eqs. (9) and (10), it is easily noticed that the use of boundary condition (9) that is successfully converted from the normal direction to the tangent direction can obtain more information from the boundary  $z = 1$  for  $\frac{\partial^2 \psi_3}{\partial z^2}$ , which will be beneficial to the fast convergence of the established algorithm. Additionally, in order to obtain the same order of accuracy for approximating  $\frac{\partial^2 \psi_3}{\partial z^2}$  at the boundary  $z = 1$ , the use of the right-hand side of Eq. (10) shall require more grid points in  $z$ -direction than Eq. (9),

which will lead to the compactness of the boundary discrete scheme to be compromised.

Now, all the boundary conditions needed, i.e.,  $\psi_i$  and  $\frac{\partial \psi_i}{\partial z}$  ( $i = 1, 2, 3$ ), are determined for the whole face  $z = 1$ . They are either directly given or obtained through known boundary conditions. In the same way, the boundary conditions of the other five faces of a cube are also determined.

## III. BASIC DISCRETE FORMULATIONS

For simplicity, consider a cube computational domain  $[0, 1]^3$ . Let  $\alpha$  stand for the independent variables  $x$ ,  $y$ , and  $z$  (similarly hereinafter), we lay out a uniform mesh  $0 = \alpha_0 < \alpha_1 < \dots < \alpha_{N_\alpha-1} < \alpha_{N_\alpha} = 1$ . Here,  $\alpha_m = mh_\alpha$ ,  $h_\alpha = \frac{1}{N_\alpha}$ , for  $m \in [0, N_\alpha]$ , while  $m$  represents the independent positive integer variables  $l$ ,  $j$ ,  $k$  at  $x$ -,  $y$ -, and  $z$ -directions, respectively; for example,  $z_k = kh_z$ ,  $h_z = \frac{1}{N_z}$ , for  $k \in [0, N_z]$ . Moreover, the difference operators  $\delta_\alpha$  and  $\delta_\alpha^2$  reused at the interior point  $(x_l, y_j, z_k)$  for a function  $\psi(x, y, z)$  are defined by

$$\begin{aligned} \delta_x \psi &= \frac{\psi_{l+1,j,k} - \psi_{l-1,j,k}}{2h_x}, \\ \delta_x^2 \psi &= \frac{\psi_{l+1,j,k} - 2\psi_{l,j,k} + \psi_{l-1,j,k}}{h_x^2}, \\ \delta_y \psi &= \frac{\psi_{l,j+1,k} - \psi_{l,j-1,k}}{2h_y}, \\ \delta_y^2 \psi &= \frac{\psi_{l,j+1,k} - 2\psi_{l,j,k} + \psi_{l,j-1,k}}{h_y^2}, \\ \delta_z \psi &= \frac{\psi_{l,j,k+1} - \psi_{l,j,k-1}}{2h_z}, \\ \delta_z^2 \psi &= \frac{\psi_{l,j,k+1} - 2\psi_{l,j,k} + \psi_{l,j,k-1}}{h_z^2}, \end{aligned} \quad (11)$$

where the subscripts  $l$ ,  $j$ , and  $k$  in  $\delta_\alpha \psi_{l,j,k}$  and  $\delta_\alpha^2 \psi_{l,j,k}$  are omitted. For convenience,  $f$  will be written in short for  $f_{l,j,k}$  if there is no confusion about the notations in the following. Meanwhile, in the following paragraphs, if a discretization is established for the interior points in one of the coordinate directions, the subscripts of the other coordinate directions would also be omitted. For example, for a function  $\psi$  at point  $(x_l, y_j, z_k)$ , if a discretization is performed in the  $z$ -direction, then the difference operators  $\delta_z$  and  $\delta_z^2$  in Eq. (11) are simplified as

$$\delta_z \psi = \frac{\psi_{k+1} - \psi_{k-1}}{2h_z}, \quad \delta_z^2 \psi = \frac{\psi_{k+1} - 2\psi_k + \psi_{k-1}}{h_z^2}. \quad (12)$$

Hence, if a discrete operator can be applied to all coordinate directions, we use the following expressions directly:

$$\delta_x \psi = \frac{\psi_{m+1} - \psi_{m-1}}{2h_x}, \quad \delta_x^2 \psi = \frac{\psi_{m+1} - 2\psi_m + \psi_{m-1}}{h_x^2}, \quad (13)$$

where  $\psi_m$  is recognized as the value of function  $\psi$  at  $\alpha = mh_\alpha$ ; for example,  $\psi_k$ , viz.,  $\psi(x, y, kh_z)$  or  $\psi(x, y, z_k)$ . It needs to be emphasized that the other simplified notations below are similar and will not be covered here.

In view of the characteristics of the boundary conditions described in Proposition 1 [see Eq. (3)], we try to choose  $\psi_i$  ( $i = 1, 2, 3$ ) and their first-order partial derivatives as the unknown

variables to establish high-order compact methods for the 3D incompressible flow problems. Meanwhile, as the basis of the construction of fourth-order compact schemes for Eq. (3), we could directly utilize the fourth- and sixth-order Padé compact difference schemes with boundary conditions for the first-order partial derivatives developed in the literature,<sup>38</sup> which are provided in the Appendix.

## A. Approximations of higher-order partial derivatives

Now, some fourth-order compact schemes would be deduced for higher partial derivatives in the streamfunction formulations involving Eqs. (4)–(6), which are based on the approximations suggested for the first partial derivatives<sup>38</sup> (see the Appendix for more detail).

### 1. Approximation of second-order partial derivatives

Considering some pure and mixed second-order partial derivatives that appeared in the pure streamfunction formulation, the fourth-order compact schemes would be provided for the pure and mixed second-order partial derivatives of  $\psi_i$  ( $i = 1, 2, 3$ ).

*a. Approximation of the pure second-order partial derivatives.* For the pure second-order partial derivative  $\frac{\partial^2 \psi_i}{\partial x^2}$ , a fourth-order compact scheme would be provided. By means of the Taylor expansion, we have

$$\frac{\partial^2 \psi_i}{\partial x^2} = \delta_x^2 \psi_i - \frac{h_x^2}{12} \frac{\partial^4 \psi_i}{\partial x^4} + O(h_x^4) \quad i = 1, 2, 3. \quad (14)$$

Following Ref. 23,  $\frac{\partial^4 \psi_i}{\partial x^4}$  can be replaced by

$$\frac{\partial^4 \psi_i}{\partial x^4} = \frac{12}{h_x^2} (\delta_x \partial_x \psi_i - \delta_x^2 \psi_i) + O(h_x^2), \quad i = 1, 2, 3, \quad (15)$$

where  $\partial_x \phi$  is a simplified form of the first-order partial derivative  $\frac{\partial \phi}{\partial x}$ .

Combining Eqs. (14) and (15), one gets

$$\frac{\partial^2 \psi_i}{\partial x^2} = 2\delta_x^2 \psi_i - \delta_x \partial_x \psi_i + O(h_x^4), \quad (16)$$

noticing the fact from Eq. (A2) that

$$F_{i,x} = \partial_x \psi_i - \frac{h_x^4}{180} \frac{\partial^5 \psi_i}{\partial x^5} + O(h_x^6). \quad (17)$$

Hence,

$$\frac{\partial^2 \psi_i}{\partial x^2} = 2\delta_x^2 \psi_i - \delta_x F_{i,x} + O(h_x^4), \quad (18)$$

where  $F_{i,x}$  is determined by the fourth-order compact scheme (A2).

Using the Taylor series expansion, the truncation error of Eq. (18) is derived as follows:

$$2\delta_x^2 \psi_i - \delta_x F_{i,x} = \frac{\partial^2 \psi_i}{\partial x^2} + \frac{h_x^4}{360} \frac{\partial^6 \psi_i}{\partial x^6} + O(h_x^6), \quad i = 1, 2, 3, \quad (19)$$

which shows that the scheme (18) is of fourth-order of accuracy. Omitting the truncation error  $O(h_x^4)$  in Eq. (18), the fourth-order approximations are obtained for  $\frac{\partial^2 \psi_i}{\partial x^2}$ . It needs to be pointed out that

this approximation was also derived by other approaches (see Refs. 2, 4, 20, and 41 for details).

*b. Approximation of the mixed second-order partial derivatives.* It is seen from the streamfunction formulation that it is necessary to construct the approximation for the second-order mixed partial derivatives of streamfunction  $\frac{\partial^2 \psi_i}{\partial x \partial \beta}$ . Notice the following relationships:

$$\delta_x \delta_\beta \psi_i = \frac{\partial^2 \psi_i}{\partial x \partial \beta} + \frac{h_x^2}{6} \frac{\partial^4 \psi_i}{\partial x^3 \partial \beta} + \frac{h_\beta^2}{6} \frac{\partial^4 \psi_i}{\partial x \partial \beta^3} + O(h_x^4, h_x^2 h_\beta^2, h_\beta^4), \quad (20)$$

$$\delta_x F_{i,\beta} = \frac{\partial^2 \psi_i}{\partial x \partial \beta} + \frac{h_x^2}{6} \frac{\partial^4 \psi_i}{\partial x^3 \partial \beta} + O(h_x^4, h_x^2 h_\beta^2, h_\beta^4), \quad (21)$$

$$\delta_\beta F_{i,x} = \frac{\partial^2 \psi_i}{\partial x \partial \beta} + \frac{h_\beta^2}{6} \frac{\partial^4 \psi_i}{\partial x \partial \beta^3} + O(h_x^4, h_x^2 h_\beta^2, h_\beta^4). \quad (22)$$

Combining the above equations to eliminate the terms with  $h_x^2$  and  $h_\beta^2$ , one has

$$\frac{\partial^2 \psi_i}{\partial x \partial \beta} = \delta_x F_{i,\beta} + \delta_\beta F_{i,x} - \delta_x \delta_\beta \psi_i + O(h_x^4, h_x^2 h_\beta^2, h_\beta^4), \quad (23)$$

where  $F_{i,x}$  and  $F_{i,\beta}$  can be determined by the fourth-order compact scheme (A2).

### 2. Approximation of third-order partial derivatives

Given some third-order pure and mixed partial derivatives appear in the streamfunction formulation, the fourth-order compact schemes would be constructed for the pure and mixed third-order partial derivatives in this subsection. Without loss of generality, a general function  $\psi_i$  ( $i = 1, 2, 3$ ) would be considered.

*a. Approximation of the pure third-order partial derivatives.* For the pure third-order partial derivative  $\frac{\partial^3 \psi_i}{\partial x^3}$ , the fourth-order accuracy compact schemes are derived as follows. Taking advantage of the Taylor expansion, one obtains

$$\delta_x \psi_i = \partial_x \psi_i + \frac{h_x^2}{6} \frac{\partial^3 \psi_i}{\partial x^3} + \frac{h_x^4}{120} \frac{\partial^5 \psi_i}{\partial x^5} + O(h_x^6) \quad (24)$$

and

$$\delta_x^2 \partial_x \psi_i = \frac{\partial^3 \psi_i}{\partial x^3} + \frac{h_x^2}{6} \frac{\partial^5 \psi_i}{\partial x^5} + O(h_x^4). \quad (25)$$

Combining Eqs. (24) and (25) and eliminating the  $\frac{\partial^5 \psi_i}{\partial x^5}$  yields

$$\begin{aligned} \frac{\partial^3 \psi_i}{\partial x^3} &= \frac{3}{2h_x^2} (10\delta_x \psi_i - h_x^2 \delta_x^2 \partial_x \psi_i - 10\partial_x \psi_i) + O(h_x^4) \\ &= \frac{3}{2} \left( 10 \frac{\delta_x \psi_i - \partial_x \psi_i}{h_x^2} - \delta_x^2 \partial_x \psi_i \right) + O(h_x^4), \end{aligned} \quad (26)$$

where  $\partial_x \psi_i$  is a simplified form of the first-order partial derivative  $\frac{\partial \psi_i}{\partial x}$ . Ignoring the truncation error  $O(h_x^4)$ , a fourth-order accuracy compact scheme is derived for  $\frac{\partial^3 \psi_i}{\partial x^3}$ . Equation (26) was also derived by other techniques (see Refs. 2 and 20 for details).

Notice that the  $\partial_x \psi_i$  is the exact value of the partial derivative in Eq. (26); hence, the approximations for  $\partial_x \psi_i$  could affect the accuracy

of  $\frac{3}{2} \left( 10 \frac{\delta_x \psi_i - \partial_x \psi_i}{h_x^2} - \delta_x^2 \partial_x \psi_i \right)$ . Obviously, if  $\partial_x \psi_i$  is approximated by the fourth-order Padé compact difference scheme (A2), Eq. (26) can actually only reach the second-order of accuracy, because the term  $\frac{\delta_x \psi_i - \partial_x \psi_i}{h_x^2}$  is only second-order of accuracy. Thus,  $\partial_x \psi_i$  in  $\frac{\delta_x \psi_i - \partial_x \psi_i}{h_x^2}$  should be approximated by  $\bar{F}_{i,\alpha}$ , where  $\bar{F}_{i,\alpha}$  is determined by using the sixth-order Padé compact difference scheme (A5) with (A7). While  $\partial_x \psi_i$  in the term  $\delta_x^2 \partial_x \psi_i$  can be approximated by fourth-order accuracy  $F_{i,\alpha}$ . Consequently, the following fourth-order accuracy compact scheme for the pure third derivative  $\frac{\partial^3 \psi_i}{\partial x^3}$  is proposed as follows:

$$\frac{\partial^3 \psi_i}{\partial x^3} = \frac{3}{2} \left( 10 \frac{\delta_x \psi_i - \bar{F}_{i,\alpha}}{h_x^2} - \delta_x^2 F_{i,\alpha} \right) + O(h_x^4), \quad (27)$$

where  $\bar{F}_{i,\alpha}$  and  $F_{i,\alpha}$  are calculated using scheme (A5) with (A7) and scheme (A2) with (A4), respectively.

Using the Taylor series expansion, we find the truncation error of Eq. (27) as

$$\frac{3}{2} \left( 10 \frac{\delta_x \psi_i - \bar{F}_{i,\alpha}}{h_x^2} - \delta_x^2 F_{i,\alpha} \right) = \frac{\partial^3 \psi_i}{\partial x^3} + \frac{19 h_x^6}{37800} \frac{\partial^9 \psi_i}{\partial x^9} + O(h_x^8) \\ i = 1, 2, 3, \quad (28)$$

which shows that the scheme (27) is actually the sixth-order of accuracy.

**Remark 3.1.** The  $\partial_x \psi_i$  in the term  $\delta_x^2 \partial_x \psi_i$  was approximated by sixth-order accuracy  $\bar{F}_{i,\alpha}$  in Ref. 20; hence, Ben-Artzi *et al.*<sup>20</sup> obtained the following fourth-order accuracy compact scheme for the pure third derivative  $\frac{\partial^3 \psi_i}{\partial x^3}$ :

$$\frac{\partial^3 \psi_i}{\partial x^3} = \frac{3}{2} \left( 10 \frac{\delta_x \psi_i - \bar{F}_{i,\alpha}}{h_x^2} - \delta_x^2 \bar{F}_{i,\alpha} \right) + O(h_x^4), \quad (29)$$

where  $\bar{F}_{i,\alpha}$  is calculated using scheme (A5) with (A7).

**Remark 3.2.** In Ref. 5, the following fourth-order accuracy compact scheme for the pure third derivative  $\frac{\partial^3 \psi_i}{\partial x^3}$  was proposed:

$$\frac{\partial^3 \psi_i}{\partial x^3} = 2 \delta_x^2 F_{i,\alpha} - \delta_x S_{i,\alpha} + O(h_x^4), \quad (30)$$

where  $F_{i,\alpha}$  was calculated using scheme (A2) with (A4), while  $S_{i,\alpha}$  was solved by

$$\left( 1 + \frac{h_x^2}{12} \delta_x^2 \right) S_{i,\alpha} = \delta_x^2 \psi_i + O(h_x^4) \quad (31)$$

and its boundary closures scheme.<sup>5</sup> Compared to scheme (18), the solution of Eq. (31) is high-cost due to its implicit nature.

*b. Approximation of mixed third-order partial derivatives.* For the mixed third-order partial derivatives  $\frac{\partial^3 \psi_i}{\partial x^2 \partial \beta}$ , the use of the Taylor expansion yields

$$\frac{\partial^3 \psi_i}{\partial x^2 \partial \beta} = \delta_x^2 \partial_\beta \psi_i + \frac{h_x^2}{12} \frac{\partial^5 \psi_i}{\partial x^4 \partial \beta} + O(h_x^4), \quad (32)$$

$$\frac{\partial^3 \psi_i}{\partial x^2 \partial \beta} = \delta_x \delta_\beta \partial_x \psi_i + \frac{h_x^2}{6} \frac{\partial^5 \psi_i}{\partial x^4 \partial \beta} + \frac{h_\beta^2}{6} \frac{\partial^5 \psi_i}{\partial x^2 \partial \beta^3} + O(h_x^4, h_x^2 h_\beta^2, h_\beta^4), \quad (33)$$

$$\frac{\partial^3 \psi_i}{\partial x^2 \partial \beta} = \delta_x^2 \delta_\beta \psi_i + \frac{h_x^2}{12} \frac{\partial^5 \psi_i}{\partial x^4 \partial \beta} + \frac{h_\beta^2}{6} \frac{\partial^5 \psi_i}{\partial x^2 \partial \beta^3} + O(h_x^4, h_x^2 h_\beta^2, h_\beta^4). \quad (34)$$

Making use of Eqs. (32)–(34), one can easily obtain

$$\frac{\partial^3 \psi_i}{\partial x^2 \partial \beta} = \delta_x^2 \partial_\beta \psi_i + \delta_x^2 \delta_\beta \psi_i - \delta_x \delta_\beta \partial_x \psi_i + O(h_x^4, h_x^2 h_\beta^2, h_\beta^4). \quad (35)$$

Omitting the truncation error  $O(h_x^4, h_x^2 h_\beta^2, h_\beta^4)$ , a fourth-order accuracy compact scheme is derived for  $\frac{\partial^3 \psi_i}{\partial x^2 \partial \beta}$ . Here, the  $\partial_x \psi_i$  and  $\partial_\beta \psi_i$  are the exact value of the partial derivative.

The  $\partial_x \psi_i$  and  $\partial_\beta \psi_i$  in Eq. (35) may be approximated using either the fourth-order accuracy  $F_{i,\alpha}$  [see Eq. (A2)] or the sixth-order accuracy  $\bar{F}_{i,\alpha}$  [see Eq. (A5)], or using both of them. In the present work, the fourth-order accuracy  $F_{i,\alpha}$  is used in the term  $\delta_x \delta_\beta \partial_x \psi_i$  and the sixth-order accuracy  $\bar{F}_{i,\beta}$  is used in the term  $\delta_x^2 \partial_\beta \psi_i$ . Hence, the following fourth-order accuracy compact scheme is obtained for the mixed third derivative  $\frac{\partial^3 \psi_i}{\partial x^2 \partial \beta}$ :

$$\frac{\partial^3 \psi_i}{\partial x^2 \partial \beta} = \delta_x^2 \bar{F}_{i,\beta} + \delta_x^2 \delta_\beta \psi_i - \delta_x \delta_\beta F_{i,\alpha} + O(h_x^4, h_x^2 h_\beta^2, h_\beta^4). \quad (36)$$

**Remark 3.3.** In Ref. 20, the  $\partial_x \psi_i$  and  $\partial_\beta \psi_i$  in Eq. (35) are approximated by  $\bar{F}_{i,\alpha}$  and  $\bar{F}_{i,\beta}$ , respectively.

$$\frac{\partial^3 \psi_i}{\partial x^2 \partial \beta} = \delta_x^2 \bar{F}_{i,\beta} + \delta_x^2 \delta_\beta \psi_i - \delta_x \delta_\beta \bar{F}_{i,\alpha} + O(h_x^4, h_x^2 h_\beta^2, h_\beta^4), \quad (37)$$

where  $\bar{F}_{i,\alpha}$  and  $\bar{F}_{i,\beta}$  are of sixth-order accuracy approximations for first derivatives  $\partial_x \psi_i$  and  $\partial_\beta \psi_i$ , respectively, which can be obtained by the solution of Eq. (A5).

**Remark 3.4.** According to Ref. 5, the fourth-order accuracy approximation for the mixed third derivative  $\frac{\partial^3 \psi_i}{\partial x^2 \partial \beta}$  is as follows:

$$\frac{\partial^3 \psi_i}{\partial x^2 \partial \beta} = \delta_x^2 F_{i,\beta} - \delta_x^2 \delta_\beta \psi_i + \delta_\beta S_{i,\alpha} + O(h_x^4, h_x^2 h_\beta^2, h_\beta^4), \quad (38)$$

where  $F_{i,\beta}$  and  $S_{i,\alpha}$  can be calculated using the fourth-order accuracy schemes (A2) and (31).

For the mixed third-order partial derivatives  $\frac{\partial^3 \psi_i}{\partial y \partial y \partial z}$ , based on the similar approach used above, one obtains

$$\frac{\partial^3 \psi_i}{\partial x \partial y \partial z} = \delta_y \delta_z \partial_x \psi_i + \delta_x \delta_z \partial_y \psi_i + \delta_x \delta_y \partial_z \psi_i - 2 \delta_x \delta_y \delta_z \psi_i \\ + O(h_x^4, h_y^4, h_z^4, h_x^2 h_y^2, h_x^2 h_z^2, h_y^2 h_z^2), \quad (39)$$

where  $\partial_x \psi_i$  is approximated by the sixth-order Padé compact difference scheme (A5).

### 3. Approximation of fourth-order partial derivatives

For the streamfunction formulation of NS equations, some fourth-order pure and mixed partial derivatives, such as  $\frac{\partial^4 \psi_i}{\partial x^4}$ ,  $\frac{\partial^4 \psi_i}{\partial x^2 \partial z^2}$ ,



have to be approximated. In this subsection, some fourth-order compact schemes would be derived.

*a. Approximation of the pure fourth-order partial derivatives.* For the pure fourth-order partial derivatives, the following Stephenson scheme is considered:<sup>3,42</sup>

$$\frac{\partial^4 \psi_i}{\partial x^4} = \frac{12}{h_x^2} (\delta_x F_{i,\alpha} - \delta_x^2 \psi_i), \quad i = 1, 2, 3, \quad (40)$$

where  $F_{i,\alpha}$  stands for the fourth-order approximation of the first-order derivatives  $\frac{\partial \psi_i}{\partial x}$  ( $i = 1, 2, 3$ ), which can be provided in Eq. (A2).

Using the Taylor series expansion, the truncation error of Eq. (40) is derived as follows:

$$\frac{12}{h_x^2} (\delta_x F_{i,\alpha} - \delta_x^2 \psi_i) = \frac{\partial^4 \psi_i}{\partial x^4} - \frac{h_x^4}{720} \frac{\partial^8 \psi_i}{\partial x^8} + O(h_x^6), \quad i = 1, 2, 3, \quad (41)$$

which shows that the scheme (40) is of the fourth-order of accuracy.

*b. Approximation of mixed fourth-order partial derivatives.* For the mixed third-order partial derivatives  $\frac{\partial^3 \psi_i}{\partial x^2 \partial \beta^2}$ , the fourth-order accurate approximation would be derived as follows. Utilizing the Taylor series expansion, one has

$$\delta_x \delta_\beta^2 F_{i,\alpha} = \frac{\partial^4 \psi_i}{\partial x^2 \partial \beta^2} + \frac{h_x^2}{6} \frac{\partial^6 \psi_i}{\partial x^4 \partial \beta^2} + \frac{h_\beta^2}{12} \frac{\partial^6 \psi_i}{\partial x^2 \partial \beta^4} + O(h_x^4, h_x^2 h_\beta^2, h_\beta^4), \quad (42)$$

$$\delta_x^2 \delta_\beta F_{i,\beta} = \frac{\partial^4 \psi_i}{\partial x^2 \partial \beta^2} + \frac{h_x^2}{12} \frac{\partial^6 \psi_i}{\partial x^4 \partial \beta^2} + \frac{h_\beta^2}{6} \frac{\partial^6 \psi_i}{\partial x^2 \partial \beta^4} + O(h_x^4, h_x^2 h_\beta^2, h_\beta^4), \quad (43)$$

$$\delta_x^2 \delta_\beta^2 \psi_i = \frac{\partial^4 \psi_i}{\partial x^2 \partial \beta^2} + \frac{h_x^2}{12} \frac{\partial^6 \psi_i}{\partial x^4 \partial \beta^2} + \frac{h_\beta^2}{12} \frac{\partial^6 \psi_i}{\partial x^2 \partial \beta^4} + O(h_x^4, h_x^2 h_\beta^2, h_\beta^4). \quad (44)$$

Combining the above equations to eliminate the terms with  $h_x^2$  and  $h_\beta^2$ , one yields

$$\frac{\partial^4 \psi_i}{\partial x^2 \partial \beta^2} = -(\delta_x \delta_\beta^2 F_{i,\alpha} + \delta_x^2 \delta_\beta F_{i,\beta}) + 3\delta_x^2 \delta_\beta^2 \psi_i + O(h_x^4, h_x^2 h_\beta^2, h_\beta^4). \quad (45)$$

Here,  $F_{i,\alpha}$  and  $F_{i,\beta}$  can be determined by the fourth-order compact scheme (A2).

## B. Fourier error analysis of high-order compact schemes

In this subsection, we use Fourier error analysis to examine the dispersion of the schemes suggested in Sec. III A and compare the results against those of the existing schemes of the same order. The Fourier analysis method provides an effective insight into the resolution characteristics and accuracy of the difference scheme.<sup>38,43</sup>

Resolution characteristics are concerned with the difference between the exact and approximation values of derivatives, which, through

Fourier analysis, is reflected by the exact wavenumbers and their approximate counterparts, termed as the modified wavenumbers.

First, using the Fourier analysis, the modified wavenumbers of the present scheme (27), Ben-Artzi's scheme (29), Yu's scheme (30), and the classical 7-point explicit central scheme for the pure third-order derivatives are

$$k_i = \frac{\sin \xi (\cos \xi - 1) (7 \cos \xi + 23)}{(2 \cos \xi + 3) (\cos \xi + 2)}, \quad (46)$$

$$k_i = \frac{3 \sin \xi (\cos \xi - 1) (11 - \cos \xi)}{6 \cos \xi + 9}, \quad (47)$$

$$k_i = \frac{36 \sin \xi (\cos \xi - 1)}{(\cos \xi + 2) (\cos \xi + 5)}, \quad (48)$$

and

$$k_i = -\frac{1}{4} \sin 3\xi + 2 \sin 2\xi - \frac{13}{4} \sin \xi, \quad (49)$$

respectively, where  $\xi = k_x h_x$  is the scaled wavenumber, and  $k_i$  is the scaled modified wavenumber.

Note that the present scheme (27), Ben-Artzi's scheme (29), Yu's scheme (30), and the classical 7-point explicit central scheme, denoted as Present, Ben-Artzi,<sup>20</sup> Yu,<sup>5</sup> and Classical (wide), respectively, are of central differences; thus, there are no numerically dissipative errors. Here, the dispersion properties of these compact schemes are compared.

Figure 1 illustrates the resolution characteristics of the Present, Ben-Artzi,<sup>20</sup> Yu,<sup>5</sup> and Classical (wide) schemes. For the same difference operator length, the Present scheme provides much better resolution than the Ben-Artzi,<sup>20</sup> Yu,<sup>5</sup> and Classical (wide) schemes. Exact difference approximation corresponds to the curve line  $k_i = \xi^3$ .

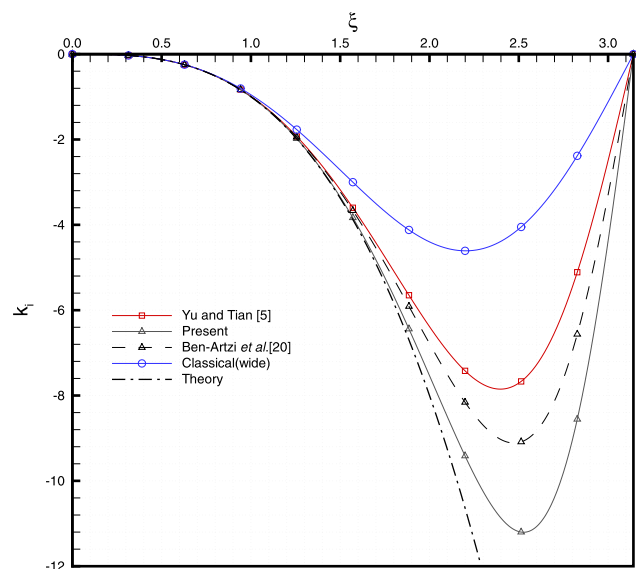


FIG. 1. Imaginary parts of modified wavenumbers of schemes for pure third-order partial derivatives  $\frac{\partial^3 \psi_i}{\partial x^2}$  as function of  $\xi = k_x h_x$ .

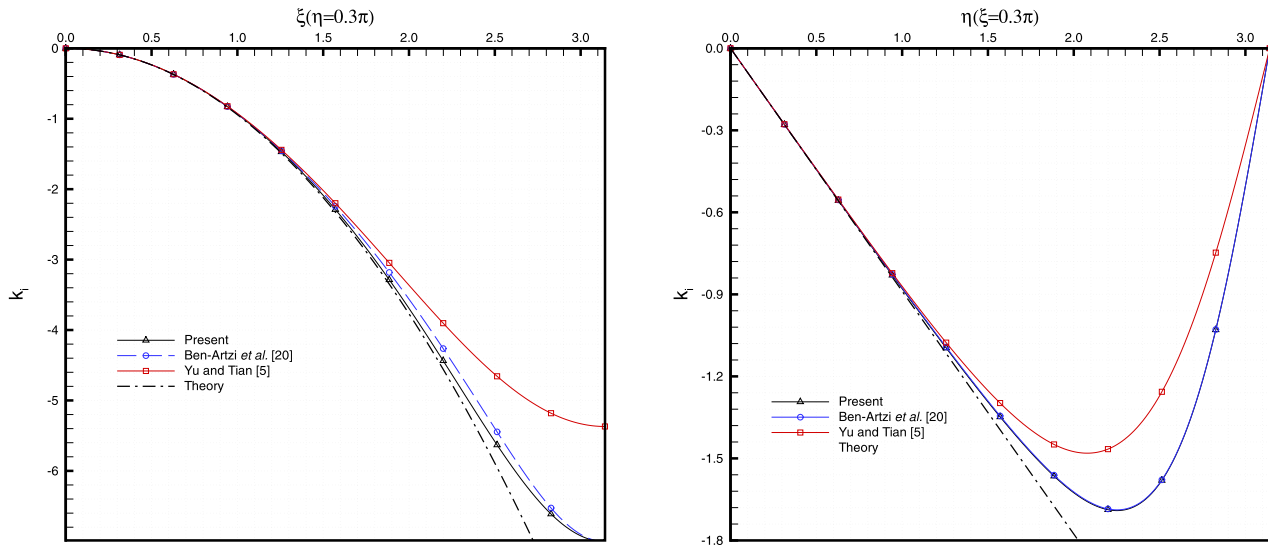


FIG. 2. Imaginary parts of modified wavenumbers of schemes for mixed third-order partial derivatives  $\frac{\partial^3 \psi_i}{\partial x^2 \partial \beta}$  as function of  $\xi = k_x h_x$  and  $\eta = k_\beta h_\beta$ .

Moreover, by the Fourier analysis, the modified wavenumbers of the mixed third-order spatial derivative by using the three compact schemes above, i.e., the Present scheme (36), Ben-Artzi's scheme (37), and Yu and Tian's scheme (38), are

$$k_i = (\cos \eta - 1) \sin \xi \left( \frac{27 \cos \xi + 23}{3 \cdot 2 \cos \xi + 3} - \frac{3 \cos \eta + 3}{\cos \eta + 2} \right), \quad (50)$$

$$k_i = \frac{1}{3} (\cos \eta - 1) \sin \xi \left[ \frac{14 \cos \xi + 46}{2 \cos \xi + 3} - \frac{(\cos \eta + 1)(\cos \eta + 14)}{2 \cos \eta + 3} \right], \quad (51)$$

and

$$k_i = 2(\cos \eta - 1) \sin \xi \left( \frac{3}{\cos \xi + 2} + \frac{6}{\cos \eta + 5} - 1 \right), \quad (52)$$

respectively, where  $\xi = k_x h_x$  and  $\eta = k_\beta h_\beta$  are the scaled wavenumbers, and  $k_i$  is the scaled modified wavenumber.

Using the Fourier analysis-based results above, the dispersion relations as function of  $\xi = k_x h_x$  and  $\eta = k_\beta h_\beta$  are plotted in Fig. 2, which show the modified wavenumbers as function of  $\eta = k_\beta h_\beta$  in the case  $\xi = 0.3\pi$  and one as function of  $\xi = k_x h_x$  in the case of  $\eta = 0.3\pi$ , respectively. Exact difference approximation corresponds to the curve line  $k_i = \xi^2 \eta$ . The Present scheme has a better resolution than the schemes given in Refs. 5 and 20, especially the scheme in Ref. 5.

Finally, using the Fourier analysis, the modified wavenumbers of the Stephenson scheme (40) and the seven-point classical explicit scheme are

$$k_r = \frac{12(\cos \xi - 1)^2}{2 + \cos \xi} \quad (53)$$

and

$$k_r = -\frac{1}{3} \cos 3\xi + 4 \cos 2\xi - 13 \cos \xi + \frac{19}{3}, \quad (54)$$

respectively, where  $\xi = k_x h_x$  is the scaled wavenumber, and  $k_r$  is the scaled modified wavenumber. Exact difference approximation corresponds to the curve line  $k_r = \xi^4$ . Figure 3 illustrates the resolution characteristics of the above two schemes. The Stephenson scheme provides higher resolution compared to the classical explicit scheme.

### C. Boundary scheme for the streamfunction

Notice that at the boundary faces,  $\psi_i$  ( $i = 1, 2, 3$ ) is not all known. For example,  $\psi_3$  is not provided directly on the boundary face.

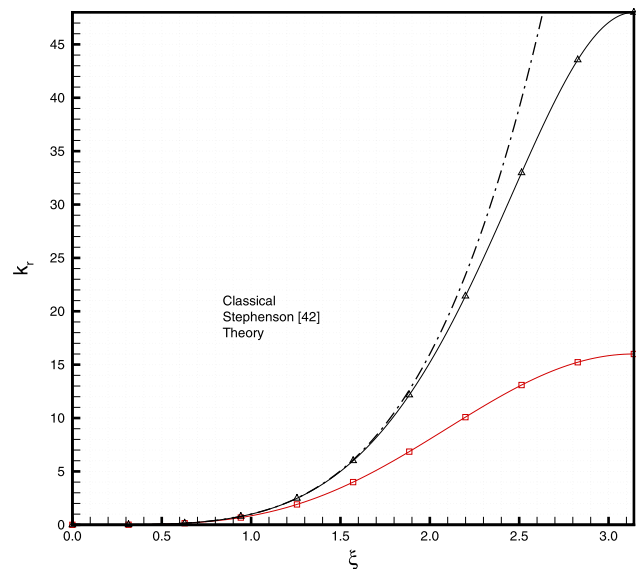


FIG. 3. Real parts of modified wavenumbers of schemes for pure fourth-order partial derivatives  $\frac{\partial^4 \psi_i}{\partial x^4}$  as function of  $\xi = k_x h_x$ .



As a result, it is necessary to establish the boundary scheme of  $\psi_3$  through other known boundary conditions associated with it. In this subsection, the boundary face  $z = 1$  is taken as an example and the numerical schemes of the streamfunction  $\psi_3$  is constructed.

Boundary conditions containing  $\frac{\partial(\nabla \cdot \psi)}{\partial n}|_{\partial\Omega} = 0$  are called as first-type boundary conditions in this work. Now, taking advantage of the known boundary conditions  $\frac{\partial\psi_3}{\partial z} = 0$  and  $\frac{\partial(\nabla \cdot \psi)}{\partial z} = 0$ , we provide the following formulation to calculate  $\psi_3$  at  $z = 1$ ,

$$(\psi_3)_{N_z} = a_1(\psi_3)_{N_z-1} + a_2(\psi_3)_{N_z-2} + bh_z \left( \frac{\partial\psi_3}{\partial z} \right)_{N_z} + ch_z^2 \left( \frac{\partial^2\psi_3}{\partial z^2} \right)_{N_z}. \quad (55)$$

Making use of the Taylor series expansion and eliminating the truncation errors of third-order and below, the coefficients are determined by

$$a_1 = \frac{8}{7}, \quad a_2 = -\frac{1}{7}, \quad b = -\frac{6}{7}, \quad c = -\frac{2}{7}. \quad (56)$$

Given the boundary conditions determined by Eq. (9) and  $\left( \frac{\partial\psi_3}{\partial z} \right)_{N_z} = 0$ , Eq. (55) can be rewritten as

$$(\psi_3)_{N_z} = \frac{8}{7}(\psi_3)_{N_z-1} - \frac{1}{7}(\psi_3)_{N_z-2} + \frac{2h_z^2}{7} \left( \frac{\partial^2\psi_3}{\partial x^2} + \frac{\partial^2\psi_3}{\partial y^2} + \frac{\partial v_b}{\partial x} - \frac{\partial u_b}{\partial y} \right)_{N_z}. \quad (57)$$

Applying Eq. (18) to Eq. (57) and eliminating  $O(h_x^4 h_z^2 + h_y^4 h_z^2)$  yields

$$(\psi_3)_{N_z} = \frac{8}{7}(\psi_3)_{N_z-1} - \frac{1}{7}(\psi_3)_{N_z-2} + \frac{4h_z^2}{7} ((\delta_x^2 + \delta_y^2)\psi_3)_{N_z} - \frac{2h_z^2}{7} (\delta_x \partial_x \psi_3 + \delta_y \partial_y \psi_3)_{N_z} + \frac{2h_z^2}{7} \left( \frac{\partial v_b}{\partial x} - \frac{\partial u_b}{\partial y} \right)_{N_z}, \quad (58)$$

namely,

$$\left( 1 - \frac{4h_z^2}{7} (\delta_x^2 + \delta_y^2) \right) (\psi_3)_{N_z} + \frac{2h_z^2}{7} (\delta_x F_{3,x} + \delta_y F_{3,y})_{N_z} = \frac{8}{7}(\psi_3)_{N_z-1} - \frac{1}{7}(\psi_3)_{N_z-2} + \frac{2h_z^2}{7} \left( \frac{\partial v_b}{\partial x} - \frac{\partial u_b}{\partial y} \right)_{N_z}, \quad (59)$$

where  $(F_{3,x})_{N_z}$  and  $(F_{3,y})_{N_z}$  are the approximate values of  $(\partial_x \psi_3)_{N_z}$  and  $(\partial_y \psi_3)_{N_z}$ , respectively, which may be calculated using the fourth-order scheme of the first derivative [see Eq. (A2)]. Thus,  $(\psi_3)_{N_z}$  and  $(F_{3,x})_{N_z}$ ,  $(F_{3,y})_{N_z}$  can be solved iteratively by using Eqs. (A2) and (59) subject to  $\psi_3 = 0$  on the edge points for the face  $z = 1$ .

It should be pointed out that the boundary scheme proposed above for  $\psi_3$  at  $z = 1$  is only established on the interior points of the face  $z = 1$ , while  $\psi_3$  on four boundaries of the face  $z = 1$  is known and equal to zero. For the other unknown  $\psi_i$  ( $i = 1, 2, 3$ ) on the boundaries, the corresponding approximations can be derived by the similar approach.

**Remark 3.5.** Compared with the boundary scheme constructed in Ref. 5, which only uses the information of the unknown variable  $\psi_3$  at the  $z$ -direction, the newly proposed boundary scheme (59) uses not only the information of the unknown variable  $\psi_3$  at the  $z$ -direction, but also the information of unknown variable  $\psi_3$  and known variables  $u_b$  and  $v_b$  for  $z = 1$  at the  $x$ - and  $y$ -directions, which would affect the convergence and efficiency of the solution. Also seen and verified in Sec. V.

## IV. NUMERICAL METHOD

In Secs. III A and III C, basic discrete formulations have been introduced for the first- and higher-order partial derivatives of the streamfunction and their boundary conditions. Now, the fourth-order compact schemes would be deduced for the streamfunction formulations involving Eqs. (4)–(6) and their boundary conditions by taking advantage of those approximations.

### A. Compact scheme for the streamfunction at the interior points

#### 1. The viscous term

The components  $V_i$  of the viscous term  $\nu \Delta^2 \psi$  in the pure streamfunction formulation (4) are

$$V_i = \nu \left( \frac{\partial^4}{\partial x^4} + \frac{\partial^4}{\partial y^4} + \frac{\partial^4}{\partial z^4} + 2 \frac{\partial^4}{\partial x^2 \partial y^2} + 2 \frac{\partial^4}{\partial x^2 \partial z^2} + 2 \frac{\partial^4}{\partial y^2 \partial z^2} \right) \psi_i, \quad i = 1, 2, 3. \quad (60)$$

Applying the fourth-order approximations (40) and (45) to (60), the following fourth-order accurate approximation for the viscous term is obtained:

$$V_i = \nu \left[ 12 \left( \frac{1}{h_x^2} (\delta_x F_{i,x} - \delta_x^2 \psi_i) + \frac{1}{h_y^2} (\delta_y F_{i,y} - \delta_y^2 \psi_i) + \frac{1}{h_z^2} (\delta_z F_{i,z} - \delta_z^2 \psi_i) \right) + 2(3(\delta_x^2 \delta_y^2 \psi_i + \delta_y^2 \delta_z^2 \psi_i + \delta_z^2 \delta_x^2 \psi_i) - (\delta_x \delta_y^2 F_{i,x} + \delta_x^2 \delta_y F_{i,y} + \delta_x \delta_z^2 F_{i,x} + \delta_x^2 \delta_z F_{i,z} + \delta_y \delta_z^2 F_{i,z} + \delta_y^2 \delta_z F_{i,y})) \right] + O(h_x^4, h_y^4, h_z^4, h_x^2 h_y^2, h_x^2 h_z^2, h_y^2 h_z^2). \quad (61)$$

#### 2. The convective term

For the pure streamfunction formulation (4), the convective term is

$$\mathbf{C} = (\mathbf{u} \cdot \nabla)(\Delta \psi - \nabla(\nabla \cdot \psi)) = \mathbf{C}_o + \mathbf{C}_s, \quad (62)$$

where  $\mathbf{C}_o = (\mathbf{u} \cdot \nabla)(\Delta \psi) = (C_{o1}, C_{o2}, C_{o3})$  and  $\mathbf{C}_s = -(\mathbf{u} \cdot \nabla) \times (\nabla(\nabla \cdot \psi)) = (C_{s1}, C_{s2}, C_{s3})$ . Substituting Eqs. (27) and (35) into Eq. (62), the following fourth-order accurate approximations for  $C_{oi}$  and  $C_{si}$  ( $i = 1, 2, 3$ ) are given:

$$\begin{aligned}
 C_{oi} = & u(\Delta_h^{yz}\bar{F}_{i,x} + \frac{3}{2}\left(10\frac{\delta_x\psi_i - \bar{F}_{i,x}}{h_x^2} - \delta_x^2 F_{i,x}\right) \\
 & + \Delta_h^{yz}\delta_x\psi_i - \delta_x\delta_y F_{i,y} - \delta_x\delta_z F_{i,z}) \\
 & + v(\Delta_h^{xz}\bar{F}_{i,y} + \frac{3}{2}\left(10\frac{\delta_y\psi_i - \bar{F}_{i,y}}{h_y^2} - \delta_y^2 F_{i,y}\right) \\
 & + \Delta_h^{xz}\delta_y\psi_i - \delta_y\delta_x F_{i,x} - \delta_y\delta_z F_{i,z}) \\
 & + w(\Delta_h^{xy}\bar{F}_{i,z} + \frac{3}{2}\left(10\frac{\delta_z\psi_i - \bar{F}_{i,z}}{h_z^2} - \delta_z^2 F_{i,z}\right) \\
 & + \Delta_h^{xy}\delta_z\psi_i - \delta_z\delta_x F_{i,x} - \delta_z\delta_y F_{i,y}) \\
 & + O(h_x^4, h_y^4, h_z^4, h_x^2 h_y^2, h_x^2 h_z^2, h_y^2 h_z^2) \quad (63)
 \end{aligned}$$

and

$$\begin{aligned}
 C_{s1} = & u(\delta_{x^3}\psi_1 + \delta_{x^2y}\psi_2 + \delta_{x^2z}\psi_3) \\
 & + v(\delta_{x^2y}\psi_1 + \delta_{y^2x}\psi_2 + \delta_{xyz}\psi_3) \\
 & + w(\delta_{x^2z}\psi_1 + \delta_{xyz}\psi_2 + \delta_{z^2x}\psi_3) \\
 & + O(h_x^4, h_y^4, h_z^4, h_x^2 h_y^2, h_x^2 h_z^2, h_y^2 h_z^2) \\
 C_{s2} = & u(\delta_{x^2y}\psi_1 + \delta_{y^2x}\psi_2 + \delta_{xyz}\psi_3) \\
 & + v(\delta_{y^2x}\psi_1 + \delta_{y^3}\psi_2 + \delta_{y^2z}\psi_3) \\
 & + w(\delta_{xyz}\psi_1 + \delta_{y^2z}\psi_2 + \delta_{z^2y}\psi_3) \\
 & + O(h_x^4, h_y^4, h_z^4, h_x^2 h_y^2, h_x^2 h_z^2, h_y^2 h_z^2) \\
 C_{s3} = & u(\delta_{x^2z}\psi_1 + \delta_{xyz}\psi_2 + \delta_{z^2x}\psi_3) \\
 & + v(\delta_{xyz}\psi_1 + \delta_{y^2z}\psi_2 + \delta_{z^2y}\psi_3) \\
 & + w(\delta_{z^2x}\psi_1 + \delta_{z^2y}\psi_2 + \delta_{z^3}\psi_3) \\
 & + O(h_x^4, h_y^4, h_z^4, h_x^2 h_y^2, h_x^2 h_z^2, h_y^2 h_z^2),
 \end{aligned} \quad (64)$$

where  $\Delta_h^{\alpha\beta} = \delta_\alpha^2 + \delta_\beta^2$ , and the difference symbolic operators such as  $\delta_{x^2y}$ ,  $\delta_{x^3}$ , and  $\delta_{xyz}$  are defined as follows:

$$\begin{aligned}
 \delta_{\alpha^2\beta}\psi_i &= \delta_\alpha^2\bar{F}_{i,\beta} + \delta_\alpha^2\delta_\beta\psi_i - \delta_\alpha\delta_\beta F_{i,\alpha} \\
 \delta_{\alpha^3}\psi_i &= \frac{3}{2}\left(10\frac{\delta_\alpha\psi_i - \bar{F}_{i,\alpha}}{h_\alpha^2} - \delta_\alpha^2 F_{i,\alpha}\right) \quad (65)
 \end{aligned}$$

$$\delta_{xyz}\psi_i = \delta_y\delta_z\bar{F}_{i,x} + \delta_x\delta_z\bar{F}_{i,y} + \delta_x\delta_y\bar{F}_{i,z} - \delta_x\delta_y\delta_z\psi_i,$$

in which  $F_{i,\alpha}$  and  $\bar{F}_{i,\alpha}$  would be calculated by the determined fourth-order compact scheme (A2) with (A4) and the sixth-order scheme (A5) with (A7), respectively.

Thus, omitting the truncation error terms, the fourth-order approximations for the convective term  $\mathbf{C} = (C_1, C_2, C_3)$  can be established with  $C_i = C_{oi} + C_{si}$  ( $i = 1, 2, 3$ ), where  $C_{oi}$  and  $C_{si}$  are approximated by Eqs. (63) and (64).

**Remark 4.1.** The approximation proposed above for the convective term  $\mathbf{C}$  consists of  $\mathbf{C}_o$  and  $\mathbf{C}_s$ . When  $\mathbf{C}_s$  is omitted,  $\mathbf{C} = \mathbf{C}_o$ , which can be used in the simplified and the modified formulations [see Eqs. (5) and (6)].

### 3. The vortex-stretching term

The vortex-stretching term of the pure streamfunction formulation (4) is

$$\begin{aligned}
 \mathbf{T} &= ((\Delta\psi - \nabla(\nabla \cdot \psi)) \cdot \nabla)(\nabla \times \psi) \\
 &= ((\Delta\psi - \nabla(\nabla \cdot \psi)) \cdot \nabla)\mathbf{u} \\
 &= (T_{o1}, T_{o2}, T_{o3}) + (T_{s1}, T_{s2}, T_{s3}), \quad (66)
 \end{aligned}$$

in which

$$(T_{o1}, T_{o2}, T_{o3}) = \left(\Delta\psi_1 \frac{\partial}{\partial x} + \Delta\psi_2 \frac{\partial}{\partial y} + \Delta\psi_3 \frac{\partial}{\partial z}\right)(u, v, w) \quad (67)$$

and

$$\begin{aligned}
 (T_{s1}, T_{s2}, T_{s3}) = & -\left(\frac{\partial(\nabla \cdot \psi)}{\partial x} \frac{\partial}{\partial x} + \frac{\partial(\nabla \cdot \psi)}{\partial y} \frac{\partial}{\partial y} \right. \\
 & \left. + \frac{\partial(\nabla \cdot \psi)}{\partial z} \frac{\partial}{\partial z}\right)(u, v, w). \quad (68)
 \end{aligned}$$

Making use of the relation  $\mathbf{u} = \nabla \times \psi$ , the first-order partial derivatives of the velocities ( $u, v, w$ ) in Eqs. (67) and (68) can be replaced with the second-order partial derivatives of the streamfunction. Thus, taking advantage of the fourth-order approximations introduced in Eqs. (18) and (23), the following fourth-order accurate approximation of  $T_{oi}$  ( $i = 1, 2, 3$ ) can be obtained:

$$\begin{aligned}
 T_{oi} = & (\nabla_h^2\psi_1)A_{i,x} + (\nabla_h^2\psi_2)A_{i,y} + (\nabla_h^2\psi_3)A_{i,z} \\
 & + O(h_x^4, h_y^4, h_z^4, h_x^2 h_y^2, h_x^2 h_z^2, h_y^2 h_z^2). \quad (69)
 \end{aligned}$$

Here,  $A_{i,\alpha}$  represents the fourth-order accurate approximation of  $\frac{\partial v_i}{\partial \alpha}$ , which ( $v_1, v_2, v_3$ ) stands for ( $u, v, w$ ), for example,

$$\begin{aligned}
 A_{1,x} &= \delta_x F_{3,y} + \delta_y F_{3,x} - \delta_x \delta_y \psi_3 - \delta_x F_{2,z} - \delta_z F_{2,x} + \delta_x \delta_z \psi_2, \\
 A_{2,x} &= \delta_x F_{1,z} + \delta_z F_{1,x} - \delta_x \delta_z \psi_1 - 2\delta_x^2 \psi_3 + \delta_x F_{3,x}, \\
 A_{3,x} &= 2\delta_x^2 \psi_2 - \delta_x F_{2,x} - \delta_x F_{1,y} - \delta_y F_{1,x} + \delta_x \delta_y \psi_1
 \end{aligned} \quad (70)$$

and

$$\nabla_h^2\psi_i = 2\Delta_h\psi_i - \delta_x F_{i,x} - \delta_y F_{i,y} - \delta_z F_{i,z}, \quad i = 1, 2, 3, \quad (71)$$

where  $\Delta_h = \delta_x^2 + \delta_y^2 + \delta_z^2$ . Using Eqs. (18) and (23), the following fourth-order accurate approximations for  $T_{si}$  ( $i = 1, 2, 3$ ) are introduced:

$$T_{si} = -W_1 A_{i,x} - W_2 A_{i,y} - W_3 A_{i,z} + O(h_x^4, h_y^4, h_z^4, h_x^2 h_y^2, h_x^2 h_z^2, h_y^2 h_z^2), \quad (72)$$

where

$$\begin{aligned}
 W_1 &= 2\delta_x^2\psi_1 - \delta_x F_{1,x} + \delta_x F_{2,y} + \delta_y F_{2,x} \\
 &\quad - \delta_x \delta_y \psi_2 + \delta_x F_{3,z} + \delta_z F_{3,x} - \delta_x \delta_z \psi_3 \\
 W_2 &= \delta_x F_{1,y} + \delta_y F_{1,x} - \delta_x \delta_y \psi_1 + 2\delta_y^2\psi_2 \\
 &\quad - \delta_y F_{2,y} + \delta_y F_{3,z} + \delta_z F_{3,y} - \delta_y \delta_z \psi_3 \\
 W_3 &= \delta_x F_{1,z} + \delta_z F_{1,x} - \delta_x \delta_z \psi_1 + \delta_y F_{2,z} \\
 &\quad + \delta_z F_{2,y} - \delta_y \delta_z \psi_2 + 2\delta_z^2\psi_3 - \delta_z F_{3,z}.
 \end{aligned} \quad (73)$$

In the end, the fourth-order accuracy approximation for the stretching term is

$$T_i = T_{oi} + T_{si} \\ = (\nabla_h^2 \psi_1 - W_1) A_{i,x} + (\nabla_h^2 \psi_2 - W_2) A_{i,y} + (\nabla_h^2 \psi_3 - W_3) A_{i,z} \\ + O(h_x^4, h_y^4, h_z^4, h_x^2 h_y^2, h_x^2 h_z^2, h_y^2 h_z^2), \quad i = 1, 2, 3. \quad (74)$$

**Remark 4.2.** The approximation proposed above for the vortex-stretching term  $T$  consists of  $T_o$  and  $T_s$ . When  $T_s$  is omitted,  $T = T_o$ , which can be used in the simplified formulation [see Eq. (5)].

#### 4. To summarize

Collecting the discretizations introduced above for the viscous, convective, and vortex-stretching terms, we have

$$\left( \frac{1}{h_x^2} \delta_x^2 \psi_i + \frac{1}{h_y^2} \delta_y^2 \psi_i + \frac{1}{h_z^2} \delta_z^2 \psi_i \right) \\ = \left[ 12 \left( \frac{1}{h_x^2} \delta_x F_{i,x} + \frac{1}{h_y^2} \delta_y F_{i,y} + \frac{1}{h_z^2} \delta_z F_{i,z} \right) \right. \\ + 2(3(\delta_x^2 \delta_y^2 \psi_i + \delta_y^2 \delta_z^2 \psi_i + \delta_z^2 \delta_x^2 \psi_i) \\ \times (\delta_x \delta_y^2 F_{i,x} + \delta_x^2 \delta_y F_{i,y} + \delta_x \delta_z^2 F_{i,x} \\ + \delta_x^2 \delta_z F_{i,z} + \delta_y^2 \delta_z F_{i,z} + \delta_y \delta_z^2 F_{i,y})) \\ \left. - Re(C_{oi} + C_{si} - T_{oi} - T_{si}) \right. \\ \left. + O(h_x^4, h_y^4, h_z^4, h_x^2 h_y^2, h_x^2 h_z^2, h_y^2 h_z^2), \quad i = 1, 2, 3. \quad (75) \right]$$

When the truncation error is omitted, Eq. (75) is the fourth-order compact scheme for the pure streamfunction formulation (4).

The system of equations arising from the scheme (75) with the boundary approximations including BC1 scheme (59) can be rewritten in a matrix form as

$$\mathbf{A} \psi_i = \mathbf{b}(\psi_i, F_{i,x}, \bar{F}_{i,x}), \quad (76)$$

where  $\mathbf{A}$  is a coefficient matrix formed by the coefficients in the left-hand side of Eq. (75).

**Remark 4.3.** If  $C_{si}$  and  $T_{si}$  are removed from Eq. (75), then the fourth-order compact scheme is one for the simplified formulation (5). If  $C_{si}$  is only removed from Eq. (75), the fourth-order scheme for the modified formulation (6) would be obtained.

#### B. Solution of algebraic systems

Given some terms with streamfunction appear in the right hand of Eq. (75), the iterative method could be utilized to solve the system of equations. In this work, the inner-outer iteration procedure is used to solve the systems of Eq. (76). In the inner iteration, the first-order partial derivatives are directly solved because their approximations are tridiagonal linear systems. In addition, the multigrid method is employed to improve the convergence of the solution of the sparse linear systems of Eq. (76).

Now, the detailed procedure of the proposed algorithm is given. Suppose  $\psi_i^n$ ,  $u_i^n$ ,  $F_{i,x}^n$ , and  $\bar{F}_{i,x}^n$  are known at the whole domain, the solutions of  $\psi_i^{n+1}$ ,  $u_i^{n+1}$ ,  $F_{i,x}^{n+1}$ , and  $\bar{F}_{i,x}^{n+1}$  are obtained by the following iterative procedure:

- (i) Calculate the right hand terms of the compact scheme of streamfunction (75) by  $\psi_i^n$ ,  $u_i^n$ ,  $F_{i,x}^n$ , and  $\bar{F}_{i,x}^n$ .
- (ii) Solve the linear system of Eq. (76) by the multigrid method with a V(3,3) circle algorithm to obtain  $\psi_i^{n+1}$  in the interior points. Here, we utilize a relaxation parameter  $\lambda$  inside the inner iteration cycles for  $\psi_i$  such as  $\psi_i^{n+1} = \lambda \psi_i^n + (1 - \lambda) \psi_i^{n+1}$ .
- (iii) Compute the right hand terms of the boundary conditions (7) to update the numerical boundary conditions.
- (iv) Determine the streamfunction  $\psi_i^{n+1}$  on the boundaries using the boundary scheme (59).
- (v) Utilize the basic discrete formulations in Sec. III A to obtain all the first-order partial derivatives of the streamfunction ( $F_{i,x}^{n+1}$  and  $\bar{F}_{i,x}^{n+1}$ ).
- (vi) Obtain the velocities  $u_i^{n+1}$  according to the relationship with the first-order partial derivatives of streamfunction.
- (vii) Repeat steps (i)–(vi), which constitute the inner iteration from  $n = 0, 1, 2, \dots$  until the maximum of  $|\psi_i^{n+1} - \psi_i^n|$  is smaller than a certain convergence criterion.

In this paper, all numerical computations are run on a Lenovo machine (Xeon E5606) with 4 GB of memory using double precision arithmetic.

#### V. NUMERICAL EXPERIMENTS

In this section, the three test problems are solved to verify the correction of our computer code and the accuracy, efficiency, and convergence of the proposed method. The numerical results obtained are also compared with the exact solutions and those using other available methods in the literature.

For convenience, the physics-preserving, the modified, and the simplified pure streamfunction formulations-based fourth-order compact schemes proposed are denoted by Scheme-P, Scheme-M, and Scheme-S, respectively, while Proposition 1-based numerical boundary schemes [see Eq. (59)] are briefly called as BC1 hereafter.

#### A. Test problem with an exact solution

Consider a test problem with the following exact solution:

$$\begin{aligned} \psi_1 &= \sin \pi y \sin \pi z, \\ \psi_2 &= \sin \pi x \sin \pi z, \\ \psi_3 &= \sin \pi x \sin \pi y \end{aligned} \quad (77)$$

in a cubic closure of  $[0, 1]^3$ . Thus,

$$\begin{aligned} u &= \pi \sin \pi x (\cos \pi y - \cos \pi z), \\ v &= \pi \sin \pi y (\cos \pi z - \cos \pi x), \\ w &= \pi \sin \pi z (\cos \pi x - \cos \pi y). \end{aligned} \quad (78)$$

This solution is consistent with no in-flow and out-flow boundary condition assumptions<sup>5</sup> and also satisfies the conditions in Proposition 1. Only the tangential velocities are given on the boundaries in this test.

The numerical tests are executed, and the convergence rates are calculated with the maximal errors of different mesh sizes. The convergence criterion is set as  $10^{-12}$  for this problem. The maximal errors of  $\psi_1$  at different mesh sizes and their calculated convergence rates are listed in Table I. The results show that Scheme-P, Scheme-M, and

**TABLE I.** Numerical results of the test problem with different grid sizes for  $Re = 10$ .

Scheme	Grid size	Maximal error	Rate	$ \nabla \cdot \psi _{\max}$	Rate	CPU time (s)
Scheme-P	$9 \times 9 \times 9$	$3.263 \times 10^{-4}$		$1.286 \times 10^{-3}$		0.71
	$17 \times 17 \times 17$	$1.180 \times 10^{-5}$	4.789	$8.035 \times 10^{-5}$	4.000	27.08
	$33 \times 33 \times 33$	$4.990 \times 10^{-7}$	4.563	$5.064 \times 10^{-6}$	3.988	1505.15
Scheme-M	$9 \times 9 \times 9$	$3.009 \times 10^{-4}$		$1.288 \times 10^{-3}$		0.90
	$17 \times 17 \times 17$	$1.156 \times 10^{-5}$	4.676	$8.119 \times 10^{-5}$	4.079	30.06
	$33 \times 33 \times 33$	$5.062 \times 10^{-7}$	4.267	$5.071 \times 10^{-6}$	4.030	1647.92
Scheme-S	$9 \times 9 \times 9$	$2.958 \times 10^{-4}$		$1.289 \times 10^{-3}$		1.05
	$17 \times 17 \times 17$	$1.157 \times 10^{-5}$	4.676	$8.165 \times 10^{-5}$	3.981	29.98
	$33 \times 33 \times 33$	$5.134 \times 10^{-7}$	4.494	$5.073 \times 10^{-6}$	4.009	1663.44
Yu-modified <sup>5</sup>	$9 \times 9 \times 9$	$2.772 \times 10^{-4}$		$1.451 \times 10^{-3}$		2.16
	$17 \times 17 \times 17$	$1.396 \times 10^{-5}$	4.313	$1.066 \times 10^{-4}$	3.767	139.35
	$33 \times 33 \times 33$	$8.892 \times 10^{-7}$	3.992	$6.975 \times 10^{-6}$	3.933	10 692.35

Scheme-S with BC1s can achieve theoretical convergence rate, which is approximately 4. Meanwhile, the max values of  $|\nabla \cdot \psi|$  are also listed in Table I. It can be seen that the values of discrete  $\nabla \cdot \psi$ , while not strictly being zero, is close to zero with fourth-order accuracy. This means that three schemes can approximately ensure  $\nabla \cdot \psi = 0$  with fourth-order accuracy, but  $\nabla \cdot \psi = 0$  cannot be strictly guaranteed under the discretized boundary condition  $\vec{n} \cdot \nabla(\nabla \cdot \psi) = 0$  [see Eq. (59)]. Therefore, retaining a discrete form of  $\nabla \cdot \psi$  in the convective and the vortex-stretching terms of the discrete equations is not only reasonable in numerical approximation, but more importantly, it also reduces the physics-informed loss.

Furthermore, to fully evaluate the performance of the proposed schemes, the computing central processing unit (CPU) times are also given in Table I. It is easily found that the computation time taken by Scheme-P with BC1 is close to or even less than that taken by Scheme-M or Scheme-S with BC1. Meantime, the results obtained by Yu and Tian's method based on the modified streamfunction formulation<sup>5</sup> using the BC1, termed as Yu-modified hereafter, are also listed in Table I. It can be seen that the present methods involving Scheme-P, Scheme-M, and Scheme-S with BC1 is more efficient compared to Yu and Tian's method<sup>5</sup> with comparable accuracy.

In conclusion, considering the overall advantages of efficiency and accuracy, the present Scheme-P with BC1 might be a better choice to solve the 3D NS equations in the pure streamfunction formulation in comparison with available paper published.<sup>5</sup>

## B. Standard lid-driven cavity flow

As a classic 3D viscous flow benchmark problem, the standard lid-driven cavity flow has been solved by many researchers in recent decades.<sup>5,7-9,44,45</sup> Some benchmark solutions for different Reynolds numbers have been obtained to demonstrate the accuracy and the effectiveness of the proposed numerical methods. For example, Jiang *et al.*<sup>46</sup> presented a least-square finite element method and obtained numerical results at  $Re = 100, 400$ , and  $1000$  on grid sizes  $50 \times 50 \times 50$ . Shu *et al.*<sup>7</sup> proposed a high accurate global method of differential quadrature (DQ) and solved numerically this problem in primitive variable form on a non-staggered grid. Synchronously, the numerical results up to  $Re = 1000$  are obtained only using  $25 \times 25 \times 25$  grid sizes.

Using a Chebyshev-collocation method with spatial accuracy was better than fifth order in general, Albensoeder and Kuhlmann<sup>9</sup> provided a benchmark solution of this problem for  $Re = 1000$  on finer grid sizes of  $96 \times 96 \times 64$ . In 2010, Feldman and Gelfgat<sup>45</sup> also numerically solved this problem and found that the oscillatory instability of the flow sets in via a subcritical symmetry-breaking Hopf bifurcation at the critical Reynolds number of  $Re_{cr} \approx 1914$ . Later, Feldman and Gelfgat<sup>8</sup> developed a parallel computation method to reduce the computational costs and reported the results based on the Richardson extrapolation from the grid sizes of  $152 \times 152 \times 152$  and  $200 \times 200 \times 200$  for higher a Reynolds number.

In this subsection, to validate the correctness and feasibility of the pure streamfunction formulations and verify the accuracy and efficiency of the newly proposed methods, the standard 3D lid-driven cavity flow is solved using the Scheme-P, Scheme-M, and Scheme-S with BC1. Computations are performed for  $Re = 100, 400, 1000$ , and  $1500$  using a uniform grid of  $33 \times 33 \times 33, 49 \times 49 \times 49$  and  $65 \times 65 \times 65$ , respectively. In calculation, the iterations are stopped when the absolute error tolerance  $10^{-8}$  is achieved. The DQ solutions,<sup>7</sup> Chebyshev-collocation solutions,<sup>9</sup> Richardson extrapolation solutions,<sup>8</sup> and high-order compact streamfunction solutions<sup>5</sup> and other available solutions<sup>19,45,47</sup> are used for comparisons.

Figure 4 displays the vertical velocities on the horizontal centerline and the horizontal velocities on the vertical centerline of the square cavity with a grid size of  $49 \times 49 \times 49$  for  $Re \leq 1000$  or  $65 \times 65 \times 65$  for  $Re = 1500$ . It can be observed from Figs. 4(c) and 4(d) that the present results computed by the Scheme-P and Scheme-M are in excellent agreement with those benchmark solutions for  $Re = 100, 400, 1000$ , and  $1500$ . Especially, the results using Scheme-P or Scheme-M with BC1 are highly consistent with Feldman's result<sup>8</sup> based on the Richardson extrapolation on the fine grid sizes, while the solution using Scheme-S with BC1 seems to have obvious errors when  $Re = 1500$ . Quantitatively, the comparison of the maximal and minimal value of those velocities and the CPU times used are summarized in Tables II–IV. Obviously, numerical results computed by Scheme-P with BC1 are in excellent agreement with those from the available literature, which are sufficiently reflected in Fig. 4. These computational results reveal that the data obtained using fewer grid points are better

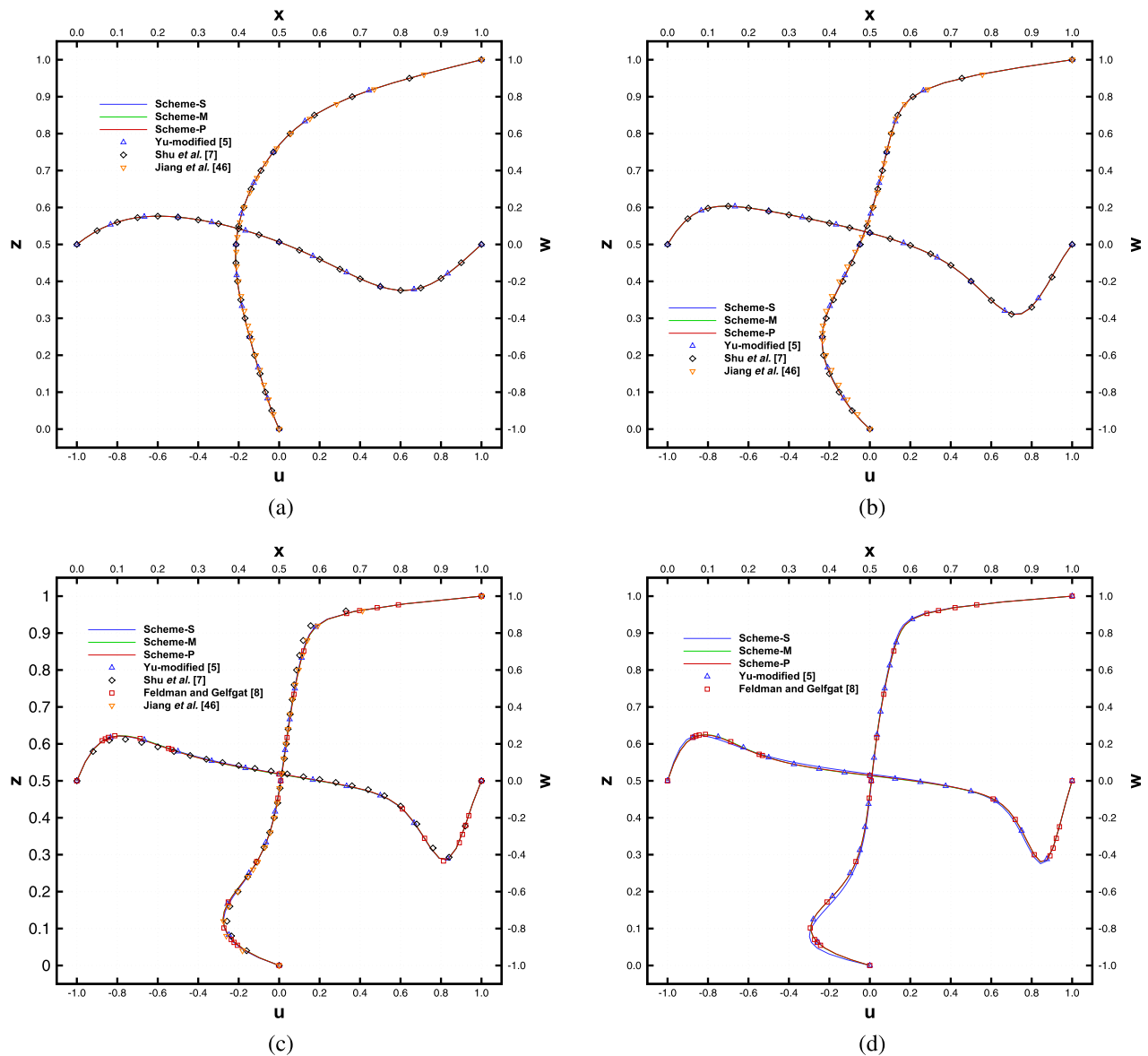


**FIG. 4.** Comparisons of the  $u$ -velocities along the line of  $(0.5, 0.5, z)$  and the  $w$ -velocities along the line of  $(x, 0.5, 0.5)$  for the standard lid-driven cavity flow at (a)  $Re = 100$ , (b)  $Re = 400$ , and (c)  $Re = 1000$  with the grid size of  $49 \times 49 \times 49$  and (d)  $Re = 1500$  with the grid size of  $65 \times 65 \times 65$ .

than those of the second-order accurate methods, such as those in Refs. 19 and 47. Additionally, it is seen from Table IV that when  $Re = 1000$ , our results using Scheme-P with the mesh size of  $49 \times 49 \times 49$  are very close to the benchmark solutions obtained by Albensoeder and Kuhlmann<sup>9</sup> with the mesh size of  $96 \times 96 \times 64$  and Feldman and Gelfgat<sup>8</sup> using finer grid points, such as the mesh size of over  $152 \times 152 \times 152$ .

Figures 5–8 provide the 3D streamline on different views using the Scheme-P with BC1 for  $Re = 100, 400, 1000$ , and  $1500$ , respectively. It is seen from the figures that there is a change in the flow patterns as the Reynolds number increases. The flow patterns are

characterized clearly by one primary and several secondary eddies from the side view of a cube cavity. For the primary eddy, the center of the eddy shifts from the upper right half region toward the cube center as the Reynolds number increases. Meanwhile, it is observed from the figures that the number of secondary eddies increases with the increase in Reynolds number. Notice from Fig. 5 that there is no evidence of the secondary eddy at  $Re = 100$ . When  $Re$  increases to 400, the downstream secondary eddy can be observed from Fig. 6. For the cases  $Re = 1000$  and  $1500$ , notice from Figs. 7 and 8, there are not only downstream secondary eddies but also upstream secondary eddies.



**TABLE II.** Comparisons of the  $u$ -velocities along the line of  $(0.5, 0.5, z)$  and the  $w$ -velocities along the line of  $(x, 0.5, 0.5)$  for the standard lid-driven cavity flow at  $Re = 100$ .

Scheme	Grid size	$u_{\min}(x, y = 0.5)$		$w_{\min}(y, z = 0.5)$		$w_{\max}(y, z = 0.5)$		Iterations	CPU time (h)
		$u$	$z$	$w$	$x$	$w$	$x$		
Scheme-P	$33 \times 33 \times 33$	-0.2156	0.4688	-0.2494	0.8125	0.1524	0.1875	14 548	0.32
	$49 \times 49 \times 49$	-0.2154	0.4792	-0.2493	0.8125	0.1529	0.2083	47 698	5.43
Scheme-M	$33 \times 33 \times 33$	-0.2150	0.4688	-0.2487	0.8125	0.1522	0.1875	14 900	0.33
	$49 \times 49 \times 49$	-0.2151	0.4792	-0.2489	0.8125	0.1528	0.2083	48 524	5.13
Scheme-S	$33 \times 33 \times 33$	-0.2150	0.4688	-0.2476	0.8125	0.1521	0.1875	15 618	0.34
	$49 \times 49 \times 49$	-0.2151	0.4792	-0.2490	0.8125	0.1529	0.2083	49 781	4.97
Yu-modified <sup>5</sup>	$33 \times 33 \times 33$	-0.2160	0.4688	-0.2487	0.8125	0.1525	0.1875	42 861	0.96
	$49 \times 49 \times 49$	-0.2156	0.4792	-0.2488	0.8125	0.1528	0.2083	151 741	15.19
Jiang <i>et al.</i> <sup>46</sup>	$50 \times 50 \times 50$	-0.2120	0.4800						
Wong and Baker <sup>19</sup>	$49 \times 49 \times 49$	-0.2154	0.4592						
Shu <i>et al.</i> <sup>7</sup>	$21 \times 21 \times 21$	-0.2140	0.4500	-0.2490	0.8000	0.1530	0.2000		
Lo <i>et al.</i> <sup>47</sup>	$51 \times 51 \times 51$	-0.2163	0.4600	-0.2617	0.8200	0.1593	0.2000		

It can be seen from Tables II–V that the computing CPU time of Scheme-P, Scheme-M, and Scheme-S with BC1 is significantly less than that for the method proposed in Ref. 5. For example, using Scheme-P with BC1 takes only 34.1%, 37.3%, 77.3%, and 66.5% of computational time by using the Yu-modified method<sup>5</sup> for cases of  $Re = 100$ , 400, 1000, and 1500 on a grid size of  $49 \times 49 \times 49$ , respectively. Meanwhile, it should be pointed out that Yu and Tian's method<sup>5</sup> also took more computational CPU time than the modified formulation-based Scheme-M with BC1, but the latter takes more CPU time than the current Scheme-P with BC1 on the same grid sizes when  $Re$

increases to 400 and 1500. All these indicate that the newly proposed Scheme-P is most suitable for solving this flow problem at  $Re \geq 400$  due to its high accuracy and low cost time consumption comparing with the other approaches used. Meanwhile, it should be pointed out that as  $Re$  increases up to 1500, Scheme-S with BC1 has the characteristics of slow convergence and visible increase in error.

### C. Diagonally lid-driven cavity flow

Consider a diagonally lid-driven cavity flow where the boundary conditions of the velocities are given by

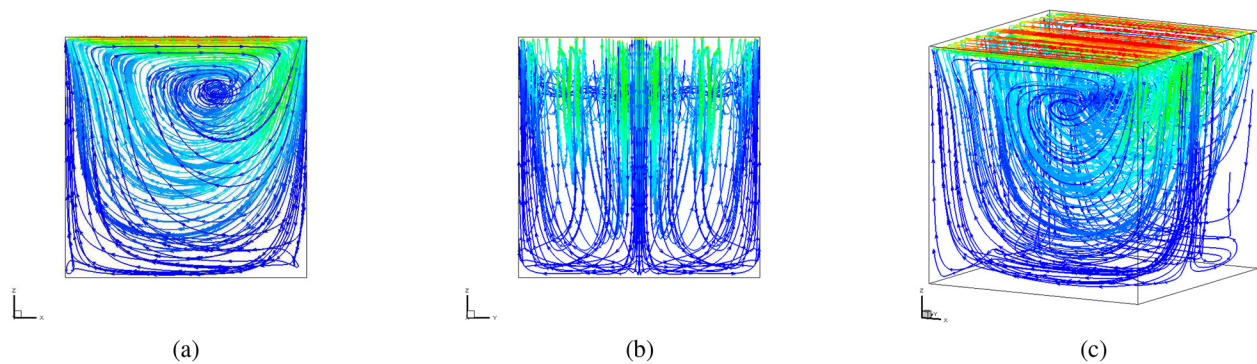
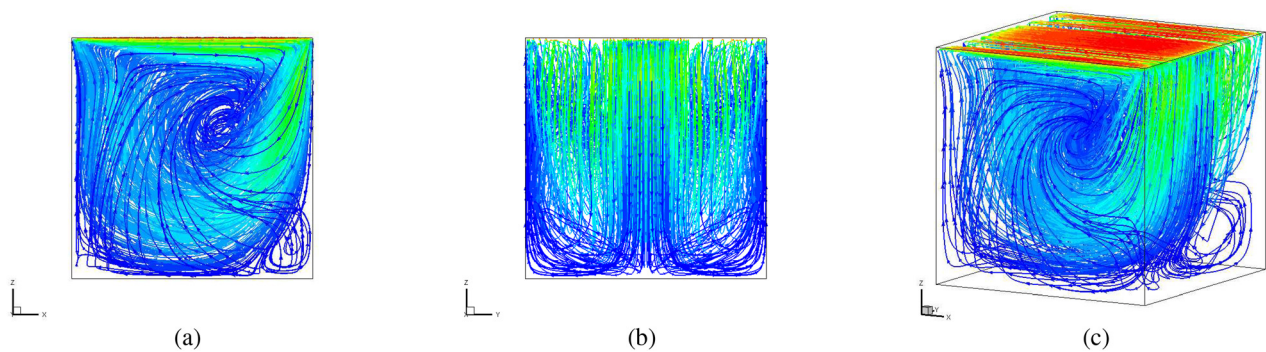
**TABLE III.** Comparisons of the  $u$ -velocities along the line of  $(0.5, 0.5, z)$  and the  $w$ -velocities along the line of  $(x, 0.5, 0.5)$  for the standard lid-driven cavity flow at  $Re = 400$ .

Scheme	Grid size	$u_{\min}(x, y = 0.5)$		$w_{\min}(y, z = 0.5)$		$w_{\max}(y, z = 0.5)$		Iterations	CPU time (h)
		$u$	$z$	$w$	$x$	$w$	$x$		
Scheme-P	$33 \times 33 \times 33$	-0.2338	0.2500	-0.3725	0.8750	0.2047	0.1563	15 496	0.37
	$49 \times 49 \times 49$	-0.2358	0.2292	-0.3791	0.8542	0.2074	0.1458	34 195	3.90
	$65 \times 65 \times 65$	-0.2365	0.2344	-0.3811	0.8594	0.2078	0.1406	81 267	17.80
Scheme-M	$33 \times 33 \times 33$	-0.2341	0.2500	-0.3719	0.8750	0.2055	0.1563	17 647	0.45
	$49 \times 49 \times 49$	-0.2354	0.2500	-0.3788	0.8542	0.2074	0.1458	37 786	4.06
	$65 \times 65 \times 49$	-0.2362	0.2344	-0.3809	0.8594	0.2077	0.1458	88 064	18.21
Scheme-S	$33 \times 33 \times 33$	-0.2326	0.2500	-0.3651	0.8750	0.2041	0.1563	20 924	0.50
	$49 \times 49 \times 49$	-0.2352	0.2500	-0.3775	0.8542	0.2068	0.1458	43 207	4.55
	$65 \times 65 \times 49$	-0.2361	0.2344	-0.3807	0.8594	0.2074	0.1458	98 067	19.43
Yu-modified <sup>5</sup>	$33 \times 33 \times 33$	-0.2343	0.2500	-0.3681	0.8750	0.2054	0.1563	28 074	0.73
	$49 \times 49 \times 49$	-0.2360	0.2500	-0.3781	0.8542	0.2076	0.1458	98 700	10.45
	$65 \times 65 \times 65$	-0.2363	0.2347	-0.3804	0.8594	0.2077	0.1406	240 840	63.05
Jiang <i>et al.</i> <sup>46</sup>	$50 \times 50 \times 50$	-0.2341	0.2600						
Wong and Baker <sup>19</sup>	$49 \times 49 \times 49$	-0.2349	0.2509						
Shu <i>et al.</i> <sup>7</sup>	$25 \times 25 \times 25$	-0.2350	0.2500	-0.3780	0.8500	0.2070	0.1500		
Lo <i>et al.</i> <sup>47</sup>	$101 \times 101 \times 101$	-0.2334	0.2600	-0.3810	0.8600	0.2010	0.1400		



**TABLE IV.** Comparisons of the  $u$ -velocities along the line of  $(0.5, 0.5, z)$  and the  $w$ -velocities along the line of  $(x, 0.5, 0.5)$  for the standard lid-driven cavity flow at  $Re = 1000$ .

Scheme	Grid size	$u_{\min}(x, y = 0.5)$		$w_{\min}(y, z = 0.5)$		$w_{\max}(y, z = 0.5)$		Iterations	CPU time (h)
		$u$	$z$	$w$	$x$	$w$	$x$		
Scheme-P	$33 \times 33 \times 33$	-0.2738	0.1250	-0.4263	0.9063	0.2379	0.0947	55 315	1.23
	$49 \times 49 \times 49$	-0.2773	0.1250	-0.4258	0.9167	0.2432	0.1042	107 564	12.52
	$65 \times 65 \times 65$	-0.2790	0.1250	-0.4321	0.9063	0.2451	0.1094	144 900	32.35
Scheme-M	$33 \times 33 \times 33$	-0.2735	0.1250	-0.4247	0.9063	0.2397	0.1250	74 810	1.67
	$49 \times 49 \times 49$	-0.2774	0.1250	-0.4256	0.9167	0.2438	0.1042	138 691	14.60
	$65 \times 65 \times 65$	-0.2790	0.1250	-0.4322	0.9063	0.2455	0.1094	176 657	35.98
Scheme-S	$49 \times 49 \times 49$	-0.2747	0.1250	-0.4256	0.9167	0.2423	0.1042	153 233	15.51
	$65 \times 65 \times 65$	-0.2774	0.1250	-0.4311	0.9063	0.2446	0.1094	203 959	42.91
Yu-modified <sup>5</sup>	$49 \times 49 \times 49$	-0.2752	0.1250	-0.4208	0.9167	0.2433	0.1042	213 435	16.20
	$65 \times 65 \times 65$	-0.2791	0.1250	-0.4317	0.9063	0.2450	0.1094	403 729	74.05
Jiang <i>et al.</i> <sup>46</sup>	$50 \times 50 \times 50$	-0.2754	0.1200						
Wong and Baker <sup>19</sup>	$49 \times 49 \times 49$	-0.2792	0.1250						
Shu <i>et al.</i> <sup>7</sup>	$31 \times 31 \times 31$	-0.2730	0.1000	-0.4290	0.9000	0.2450	0.1000		
Lo <i>et al.</i> <sup>47</sup>	$101 \times 101 \times 101$	-0.2671	0.1200	-0.4153	0.9200	0.2362	0.1000		
Albensoeder and Kuhlmann <sup>9</sup>	$97 \times 97 \times 65$	-0.2804	0.1242	-0.4350	0.9096	0.2467	0.1091		
Feldman and Gelfgat <sup>8</sup>	Extrapolation	-0.2729	0.1016	-0.4342	0.9063	0.2440	0.0938		

**FIG. 5.** 3D streamlines at  $Re = 100$  for the standard lid-driven cavity flow with the grid size of  $65 \times 65 \times 65$  on different views: (a) side view, (b) back view, and (c) oblique view.**FIG. 6.** 3D streamlines at  $Re = 400$  for the standard lid-driven cavity flow with the grid size of  $65 \times 65 \times 65$  on different views: (a) side view, (b) back view, and (c) oblique view.

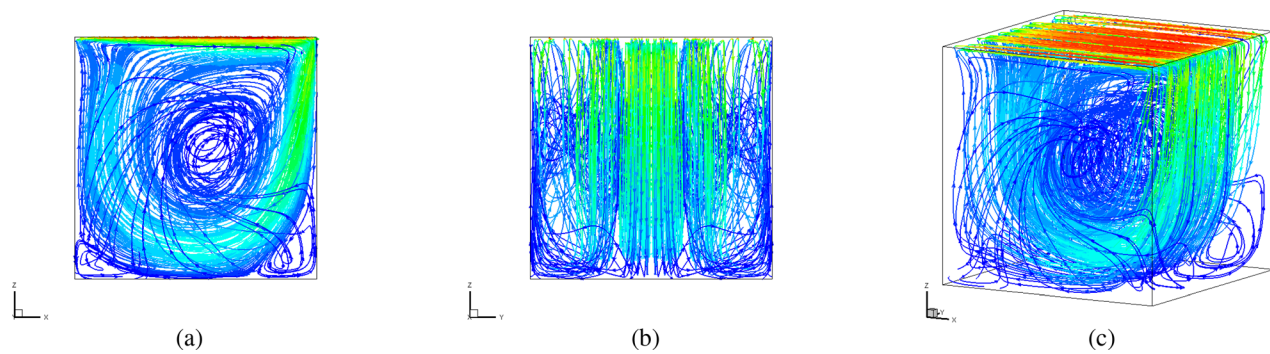


FIG. 7. 3D streamlines at  $Re = 1000$  for the standard lid-driven cavity flow with the grid size of  $65 \times 65 \times 65$  on different views: (a) side view, (b) back view, and (c) oblique view.

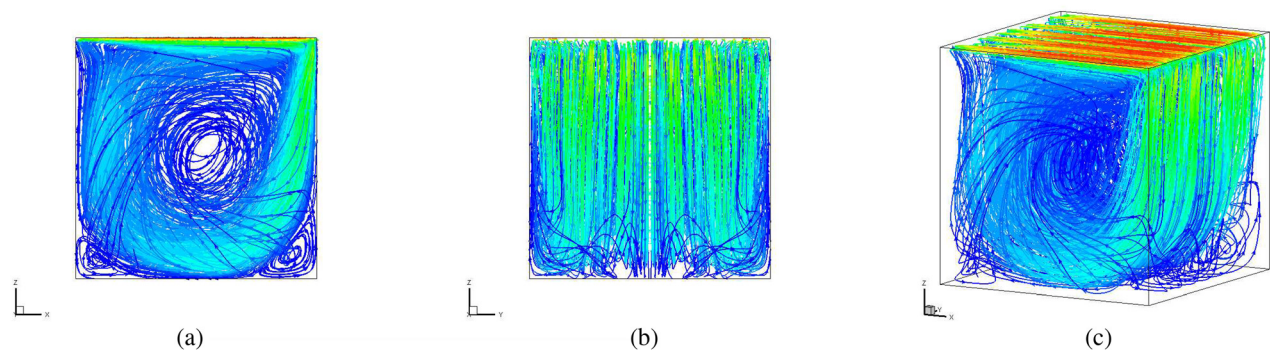


FIG. 8. 3D streamlines at  $Re = 1500$  for the standard lid-driven cavity flow with the grid size of  $65 \times 65 \times 65$  on different views: (a) side view, (b) back view, and (c) oblique view.

TABLE V. Comparisons of the  $u$ -velocities along the line of  $(0.5, 0.5, z)$  and the  $w$ -velocities along the line of  $(x, 0.5, 0.5)$  for the standard lid-driven cavity flow at  $Re = 1500$ .

Scheme	Grid size	$u_{\min}(x, y = 0.5)$		$w_{\min}(y, z = 0.5)$		$w_{\max}(y, z = 0.5)$		Iterations	CPU time (h)
		$u$	$z$	$w$	$x$	$w$	$x$		
Scheme-P	$33 \times 33 \times 33$	-0.2936	0.0938	-0.4305	0.9375	0.2485	0.0938	120 682	3.32
	$49 \times 49 \times 49$	-0.2899	0.1042	-0.4283	0.9167	0.2461	0.0833	171 816	19.87
	$65 \times 65 \times 65$	-0.2904	0.0938	-0.4376	0.9219	0.2485	0.0938	313 027	66.70
Scheme-M	$33 \times 33 \times 33$	-0.2841	0.0938	-0.4272	0.9375	0.2420	0.0938	181 181	4.55
	$49 \times 49 \times 49$	-0.2901	0.1042	-0.4279	0.9167	0.2472	0.1042	253 476	26.86
	$65 \times 65 \times 65$	-0.2914	0.0938	-0.4384	0.9219	0.2499	0.0938	427 418	88.85
Scheme-S	$65 \times 65 \times 65$	-0.2986	0.0781	-0.4486	0.9219	0.2455	0.0781	584 069	120.77
Yu-modified <sup>5</sup>	$49 \times 49 \times 49$	-0.2852	0.1042	-0.4243	0.9167	0.2453	0.1042	392 039	29.86
	$65 \times 65 \times 65$	-0.2889	0.1093	-0.4359	0.9219	0.2489	0.0938	612 460	131.09
Feldman and Gelfgat <sup>8</sup>	Extrapolation	-0.2943	0.1016	-0.4062	0.9453	0.2515	0.0938		

$$\begin{cases} u = v = \frac{\sqrt{2}}{2}, & \text{at } z = 1, \\ u = v = w = 0, & \text{else.} \end{cases} \quad (79)$$

This flow problem was first investigated by Povitsky<sup>34</sup> using FLUENT software numerically. Later, some researchers also used this

problem to assess their proposed numerical methods.<sup>5,8,36,37,48</sup> Different from the above standard lid-driven cavity flow problem, two tangential velocity components appear on the lid. In fact, the solution of this problem is more difficult because two velocity components are singular at the corner of the lid of the cavity. Consequently, it is undoubted that this problem can be utilized to evaluate the reliability,

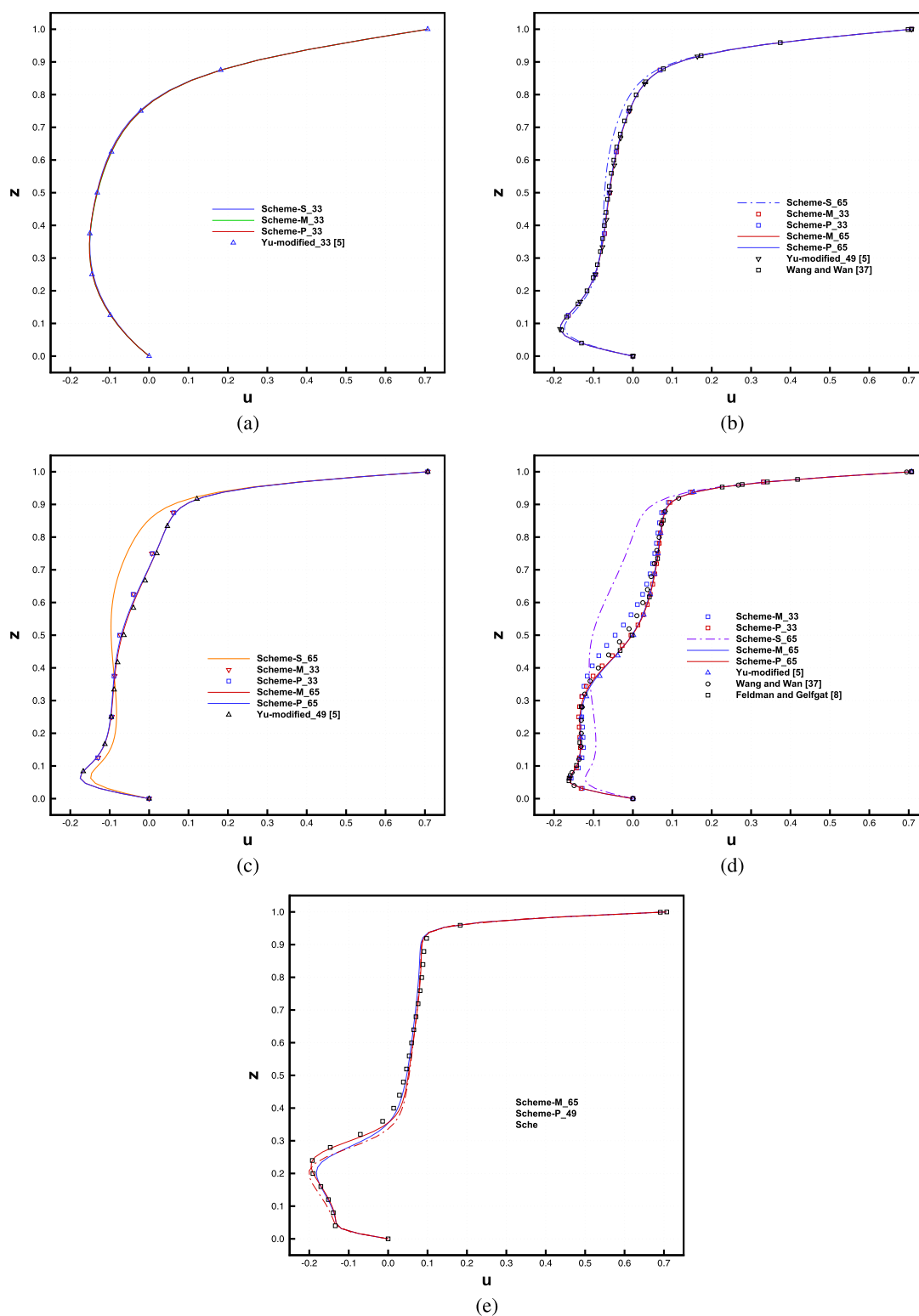


**FIG. 9.** Comparisons of the  $u$ -velocities along the line of  $(0.5, 0.5, z)$  for the diagonally lid-driven cavity flow at (a)  $Re = 100$ , (b)  $Re = 400$ , (c)  $Re = 700$ , (d)  $Re = 1000$ , and (e)  $Re = 2000$ .

**TABLE VI.** Comparisons of the  $u$ -velocities along the line of  $(0.5, 0.5, z)$  and the  $w$ -velocities along the line of  $(x, 0.5, 0.5)$  for the diagonally lid-driven cavity flow at  $Re = 100$ .

Scheme	Grid size	$u_{\min}(x, y = 0.5)$		$w_{\min}(y, z = 0.5)$		$w_{\max}(y, z = 0.5)$		Iterations	CPU time (h)
		$u$	$z$	$w$	$x$	$w$	$x$		
Scheme-P	$33 \times 33 \times 33$	-0.1515	0.3438	-0.0464	0.3438	$7.48 \times 10^{-2}$	0.7813	13 358	0.36
	$49 \times 49 \times 49$	-0.1518	0.3333	-0.0463	0.3333	$7.48 \times 10^{-2}$	0.7917	44 491	5.14
Scheme-M	$33 \times 33 \times 33$	-0.1511	0.3438	-0.0454	0.3438	$7.54 \times 10^{-2}$	0.7813	13 788	0.31
	$49 \times 49 \times 49$	-0.1516	0.3333	-0.0459	0.3333	$7.49 \times 10^{-2}$	0.7917	45 446	4.71
Scheme-S	$33 \times 33 \times 33$	-0.1505	0.3438	-0.0459	0.3438	$7.52 \times 10^{-2}$	0.7813	14 446	0.35
	$49 \times 49 \times 49$	-0.1513	0.3333	-0.0462	0.3333	$7.48 \times 10^{-2}$	0.7917	110 276	4.70
Yu-modified <sup>5</sup>	$33 \times 33 \times 33$	-0.1520	0.3438	-0.0462	0.3438	$7.53 \times 10^{-2}$	0.7813	68 139	1.34
	$49 \times 49 \times 49$	-0.1520	0.3333	-0.0461	0.3333	$7.48 \times 10^{-2}$	0.7916	122 512	12.46
Wang and Wan <sup>37</sup>	$48 \times 48 \times 48$	-0.1500	0.3197						

**TABLE VII.** Comparisons of the  $u$ -velocities along the line of  $(0.5, 0.5, z)$  and the  $w$ -velocities along the line of  $(x, 0.5, 0.5)$  for the diagonally lid-driven cavity flow at  $Re = 400$ .

Scheme	Grid size	$u_{\min}(x, y = 0.5)$		$w_{\min}(y, z = 0.5)$		$w_{\max}(y, z = 0.5)$		Iterations	CPU time (h)
		$u$	$z$	$w$	$x$	$w$	$x$		
Scheme-P	$33 \times 33 \times 33$	-0.1826	0.0938	-0.1053	0.2813	$4.29 \times 10^{-2}$	0.8438	11 168	0.29
	$49 \times 49 \times 49$	-0.1842	0.0833	-0.1050	0.2917	$4.35 \times 10^{-2}$	0.8333	29 266	3.55
	$65 \times 65 \times 65$	-0.1835	0.0938	-0.1050	0.2969	$4.36 \times 10^{-2}$	0.8438	65 467	14.56
Scheme-M	$33 \times 33 \times 33$	-0.1815	0.0938	-0.1023	0.2813	$4.65 \times 10^{-2}$	0.8438	17 741	0.40
	$49 \times 49 \times 49$	-0.1850	0.0833	-0.1030	0.2917	$3.90 \times 10^{-2}$	0.8333	39 951	4.21
	$65 \times 65 \times 65$	-0.1835	0.0938	-0.1037	0.2969	$3.59 \times 10^{-2}$	0.8438	72 065	14.92
Scheme-S	$33 \times 33 \times 33$	-0.1544	0.0938	-0.1124	0.3125	$4.26 \times 10^{-2}$	0.8438	21 644	0.47
	$49 \times 49 \times 49$	-0.1690	0.0833	-0.1121	0.3125	$4.17 \times 10^{-2}$	0.8333	44 861	4.49
	$65 \times 65 \times 65$	-0.1735	0.0938	-0.1106	0.2969	$4.21 \times 10^{-2}$	0.8438	78 448	16.15
Yu-modified <sup>5</sup>	$33 \times 33 \times 33$	-0.1839	0.0938	-0.1022	0.2813	$4.49 \times 10^{-2}$	0.8438	56 879	0.98
	$49 \times 49 \times 49$	-0.1852	0.0833	-0.1036	0.2917	$4.40 \times 10^{-2}$	0.8333	77 864	8.38
	$65 \times 65 \times 65$	-0.1840	0.0938	-0.1043	0.2969	$4.35 \times 10^{-2}$	0.8438	187 552	46.14
Wang and Wan <sup>37</sup>	$48 \times 48 \times 48$	-0.1813	0.0799						

**TABLE VIII.** Comparisons of the  $u$ -velocities along the line of  $(0.5, 0.5, z)$  and the  $w$ -velocities along the line of  $(x, 0.5, 0.5)$  for the diagonally lid-driven cavity flow at  $Re = 700$ .

Scheme	Grid size	$u_{\min}(x, y = 0.5)$		$w_{\min}(y, z = 0.5)$		$w_{\max}(y, z = 0.5)$		Iterations	CPU time (h)
		$u$	$z$	$w$	$x$	$w$	$x$		
Scheme-P	$33 \times 33 \times 33$	-0.1734	0.0625	-0.1308	0.2813	$2.94 \times 10^{-2}$	0.8750	42 538	1.02
	$49 \times 49 \times 49$	-0.1746	0.0625	-0.1273	0.2917	$3.05 \times 10^{-2}$	0.8750	87 010	10.65
	$65 \times 65 \times 65$	-0.1750	0.0625	-0.1269	0.2813	$3.07 \times 10^{-2}$	0.8750	130 178	27.50
Scheme-M	$33 \times 33 \times 33$	-0.1703	0.0625	-0.1254	0.2813	$3.14 \times 10^{-2}$	0.8750	72 213	1.78
	$49 \times 49 \times 49$	-0.1737	0.0625	-0.1246	0.2917	$3.13 \times 10^{-2}$	0.8750	118 158	12.18
	$65 \times 65 \times 65$	-0.1746	0.0625	-0.1250	0.2813	$3.11 \times 10^{-2}$	0.8750	159 826	36.58
Scheme-S	$65 \times 65 \times 65$	-0.1483	0.0625	-0.1250	0.3125	$2.28 \times 10^{-2}$	0.8906	163 746	32.56
Yu-modified <sup>5</sup>	$33 \times 33 \times 33$	-0.1742	0.0625	-0.1243	0.2813	$3.41 \times 10^{-2}$	0.8750	106 663	1.95
	$49 \times 49 \times 49$	-0.1750	0.0625	-0.1254	0.2917	$3.24 \times 10^{-2}$	0.8750	220 817	18.69
	$65 \times 65 \times 65$	-0.1751	0.0625	-0.1256	0.2917	$3.12 \times 10^{-2}$	0.8750	523 298	101.19

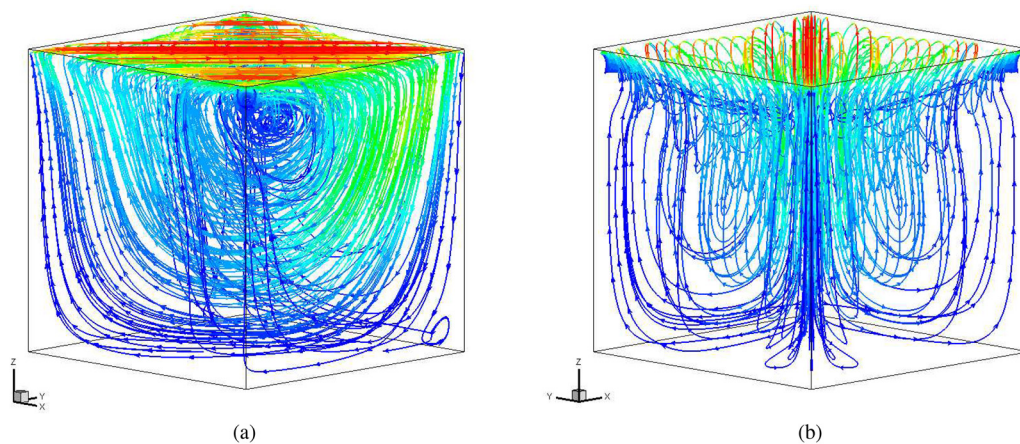


**TABLE IX.** Comparisons of the  $u$ -velocities along the line of  $(0.5, 0.5, z)$  and the  $w$ -velocities along the line of  $(x, 0.5, 0.5)$  for the diagonally lid-driven cavity flow at  $Re = 1000$ .

Scheme	Grid size	$u_{\min}(x, y = 0.5)$		$w_{\min}(y, z = 0.5)$		$w_{\max}(y, z = 0.5)$		Iterations	CPU time (h)
		$u$	$z$	$w$	$x$	$w$	$x$		
Scheme-P	$33 \times 33 \times 33$	-0.1615	0.0625	-0.1679	0.2813	$3.13 \times 10^{-2}$	0.8750	56 663	1.35
	$49 \times 49 \times 49$	-0.1602	0.0625	-0.1625	0.2708	$3.04 \times 10^{-2}$	0.8750	125 604	14.98
	$65 \times 65 \times 65$	-0.1611	0.0625	-0.1611	0.2656	$3.05 \times 10^{-2}$	0.8750	229 308	41.08
Scheme-M	$33 \times 33 \times 33$	-0.1565	0.0625	-0.1613	0.2813	$3.20 \times 10^{-2}$	0.8438	106 772	2.73
	$49 \times 49 \times 49$	-0.1592	0.0625	-0.1584	0.2708	$3.14 \times 10^{-2}$	0.8750	199 870	21.13
	$65 \times 65 \times 65$	-0.1606	0.0625	-0.1589	0.2656	$3.09 \times 10^{-2}$	0.8750	321 190	67.31
Scheme-S	$65 \times 65 \times 65$	-0.1221	0.0625	-0.1490	0.2969	$2.46 \times 10^{-2}$	0.0613	361 194	79.74
Yu-modified <sup>5</sup>	$49 \times 49 \times 49$	-0.1608	0.0625	-0.1574	0.2500	$3.30 \times 10^{-2}$	0.8542	520 773	40.40
	$65 \times 65 \times 65$	-0.1610	0.0625	-0.1596	0.2656	$3.15 \times 10^{-2}$	0.8750	641 775	112.61
Wang and Wan <sup>37</sup>	$48 \times 48 \times 48$	-0.1547	0.0799						
Feldman and Gelfgat <sup>8</sup>	Extrapolation	-0.1623	0.0547	-0.1609	0.2813	$2.98 \times 10^{-2}$	0.8516		

**TABLE X.** Comparisons of the  $u$ -velocities along the line of  $(0.5, 0.5, z)$  and the  $w$ -velocities along the line of  $(x, 0.5, 0.5)$  for the diagonally lid-driven cavity flow at  $Re = 2000$ .

Scheme	Grid size	$u_{\min}(x, y = 0.5)$		$w_{\min}(y, z = 0.5)$		$w_{\max}(y, z = 0.5)$	
		$u$	$z$	$w$	$x$	$w$	$x$
Scheme-P	$49 \times 49 \times 49$	-0.2003	0.2083	-0.2400	0.2083	$2.44 \times 10^{-2}$	0.9167
	$65 \times 65 \times 65$	-0.1930	0.2188	-0.2258	0.2344	$2.36 \times 10^{-2}$	0.9219
Scheme-M	$65 \times 65 \times 65$	-0.1821	0.2031	-0.2156	0.2188	$2.38 \times 10^{-2}$	0.9219
Yu-modified <sup>5</sup>	$65 \times 65 \times 65$	-0.1772	0.2031	-0.2117	0.2188	$2.44 \times 10^{-2}$	0.9219
Wang and Wan <sup>37</sup>	$48 \times 48 \times 48$	-0.1923	0.2398				

**FIG. 10.** 3D streamlines at  $Re = 100$  for the diagonally lid-driven cavity flow with the grid size of  $65 \times 65 \times 65$  on different oblique views: (a) perpendicular to the direction of the lid and (b) parallel to the direction of the lid.

accuracy, and robustness of the newly proposed algorithms and be employed to test the rationality of the boundary condition. For instance, a PARASA-CLGS smoother-based parallelized version of multigrid algorithm was developed by Feldman and Gelfgat<sup>8</sup> for unsteady incompressible

NS equations on staggered grids and was utilized to provide the benchmark solution of this flow problem. It should be noticed that to obtain the solution with the finest mesh size of  $200 \times 200 \times 200$ , up to 2048 cores in parallel were used in their computing. Feldman and Gelfgat<sup>35</sup> studied the

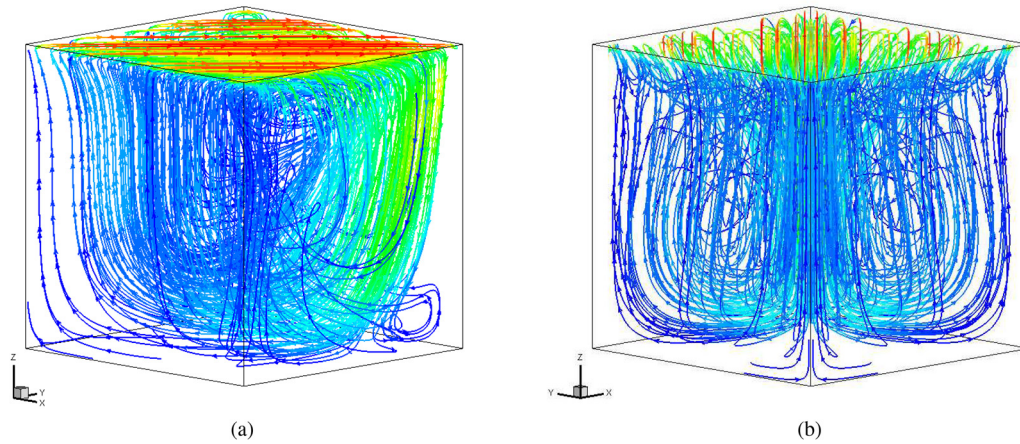


**FIG. 11.** 3D streamlines at  $Re = 400$  for the diagonally lid-driven cavity flow with the grid size of  $65 \times 65 \times 65$  on different oblique views: (a) perpendicular to the direction of the lid and (b) parallel to the direction of the lid.

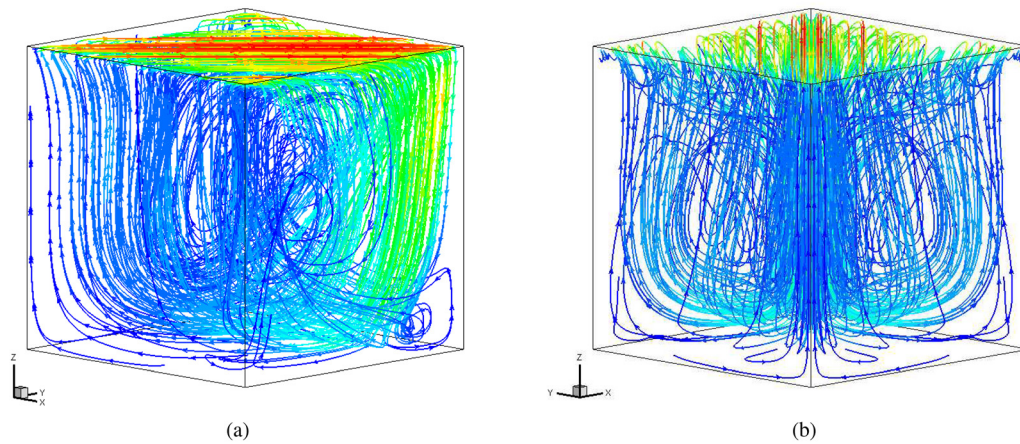


**FIG. 12.** 3D streamlines at  $Re = 700$  for the diagonally lid-driven cavity flow with the grid size of  $65 \times 65 \times 65$  on different oblique views: (a) perpendicular to the direction of the lid and (b) parallel to the direction of the lid.

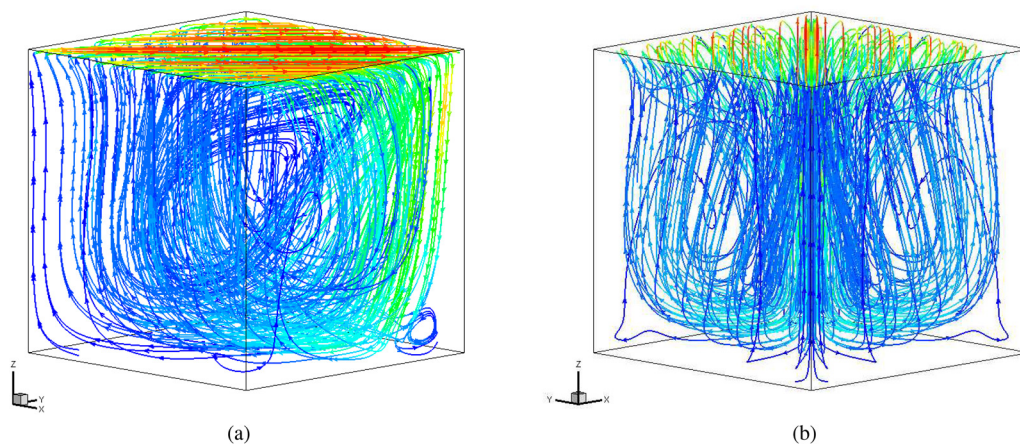


**FIG. 13.** 3D streamlines at  $Re = 1000$  for the diagonally lid-driven cavity flow with the grid size of  $65 \times 65 \times 65$  on different oblique views: (a) perpendicular to the direction of the lid and (b) parallel to the direction of the lid.



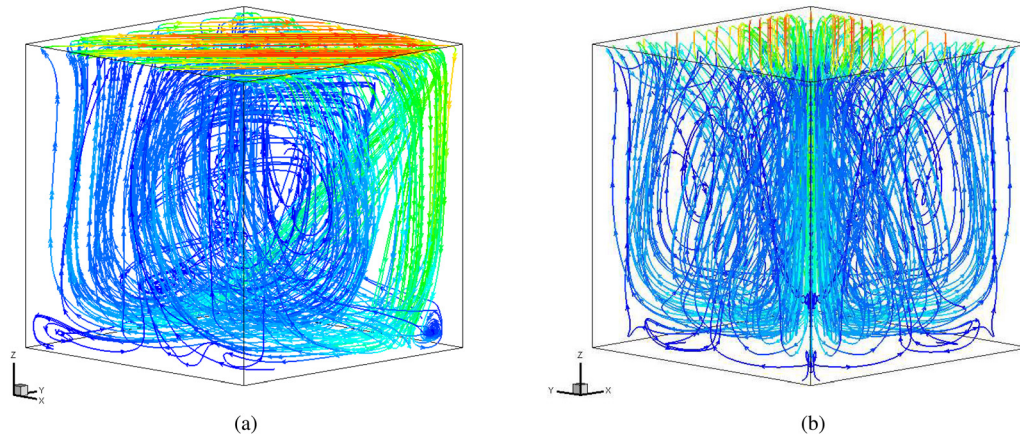


**FIG. 14.** 3D streamlines at  $Re = 2000$  for the diagonally lid-driven cavity flow with the grid size of  $65 \times 65 \times 65$  on different oblique views: (a) perpendicular to the direction of the lid and (b) parallel to the direction of the lid.

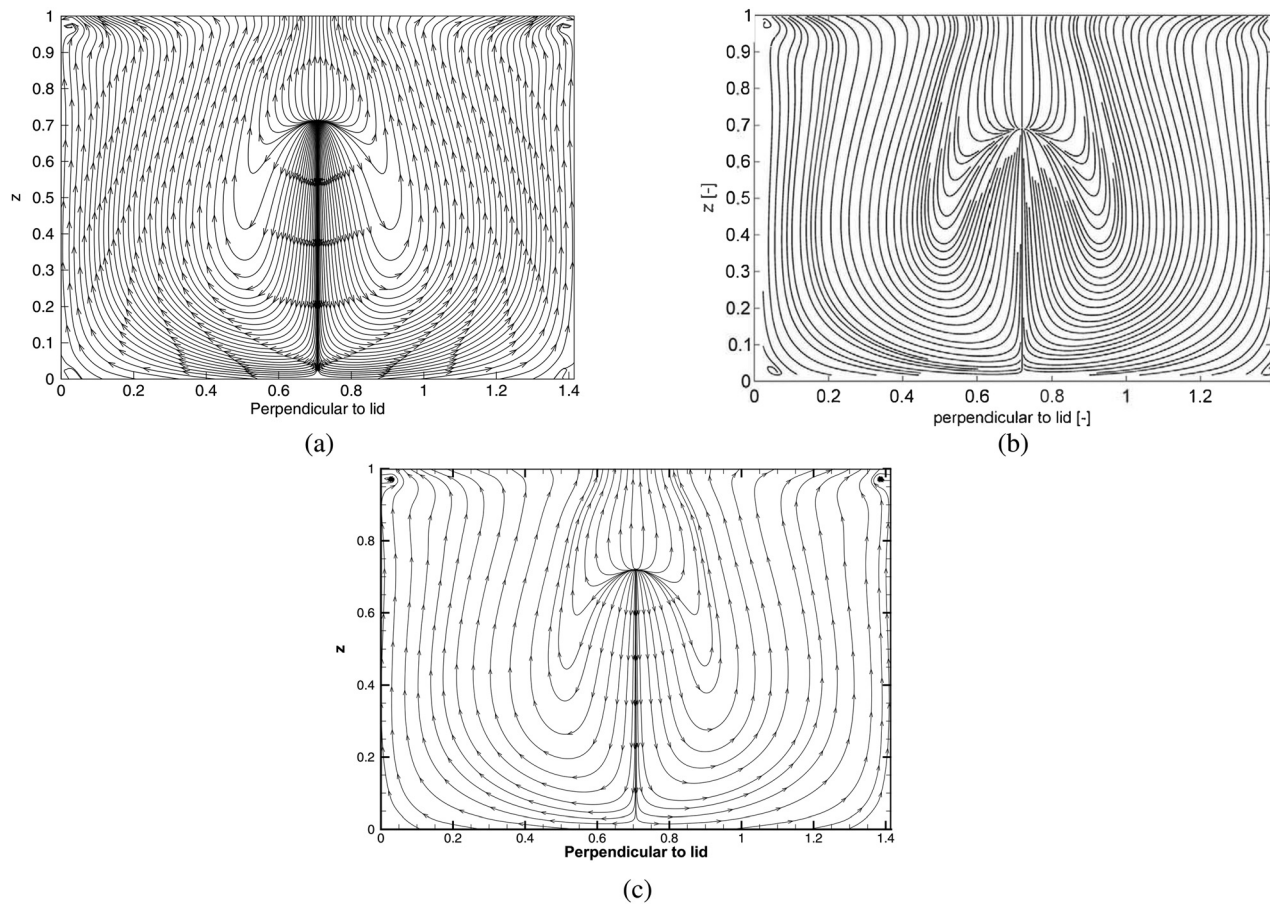


**FIG. 15.** Comparisons of the flow in the plane perpendicular to the direction of the lid ( $y = 1 - x$ ) at  $Re = 700$  for (a) our results, (b) Asinari's results,<sup>36</sup> and (c) Yu's results.

oscillatory instability and found it was set in via a subcritical symmetry breaking Hopf bifurcation, and it gave the critical value of the Reynolds number, which was around 2320. Wang and Wan<sup>37</sup> applied the fractional step finite element method (FEM) and domain decomposition method to simulate in parallel this problem for different Reynolds numbers based on the open source codes PETScFEM.<sup>49</sup>

In this subsection, the numerical experiments of diagonally lid-driven cavity flow at different Reynolds numbers  $Re$  ranging from 100 to 2000 are carried out with the convergence criterion of  $10^{-8}$ . Figure 9 exhibits the horizontal velocities on the vertical centerline of the square cavity. Notice that only when  $Re = 100$ , our numerical results with Scheme-S with BC1 can agree with those of the other present formulation and the existing results.<sup>5,37</sup> With Reynolds number increase, the differences between the data obtained by Scheme-S with BC1 even using finer mesh size of  $65 \times 65 \times 65$  and the literature results are gradually increasing, and when  $Re = 2000$ , no convergent solution can be obtained. Meanwhile, it can be noted that the data based on Scheme-M with BC1 are in good agreement with those existing results on a coarser grid size of  $33 \times 33 \times 33$  for  $Re \leq 700$ . As Reynolds numbers  $Re$  increase to 1000, the data obtained using the Scheme-M with BC1 are consistent with those in the literature if a grid size of  $65 \times 65 \times 65$  is used. Unfortunately, when the Reynolds

number  $Re$  achieves 2000, using the Scheme-M with BC1 can give a convergent solution with a grid size of  $65 \times 65 \times 65$ , but the data do not agree well with those given in the literature. However, the results calculated by the Scheme-P with BC1 only using  $33 \times 33 \times 33$  grid size are in good agreement with those in the available literature for all the Reynolds numbers  $Re \leq 1000$ , and when  $Re = 2000$ , the data calculated by the Scheme-P with BC1 with a grid size of  $65 \times 65 \times 65$  match well with those obtained in the literature, which indicates the Scheme-P with BC1 is accurate and reliable compared with Scheme-M and Scheme-S with BC1.

Quantitatively, the comparisons of the vertical velocities on the horizontal centerline and the horizontal velocities on the vertical centerline of the square cavity are tabulated in Tables VI–X. The results show that our numerical solutions based on Scheme-M with BC1 for  $Re \leq 700$  and Scheme-P with BC1 for all  $Re$  can agree with other available results well using fewer grid points, which have been reflected in Fig. 9. Additionally, the computational CPU time consumed using the present three schemes and Yu-modified method<sup>5</sup> is recorded and inserted in Tables VI–X to assess the comprehensive performance of numerical methods suggested. In cases  $Re \geq 400$ , Scheme-P with BC1 takes the least amount of computing CPU time. For example, compared to Yu-modified method with BC1<sup>5</sup> at a grid size of

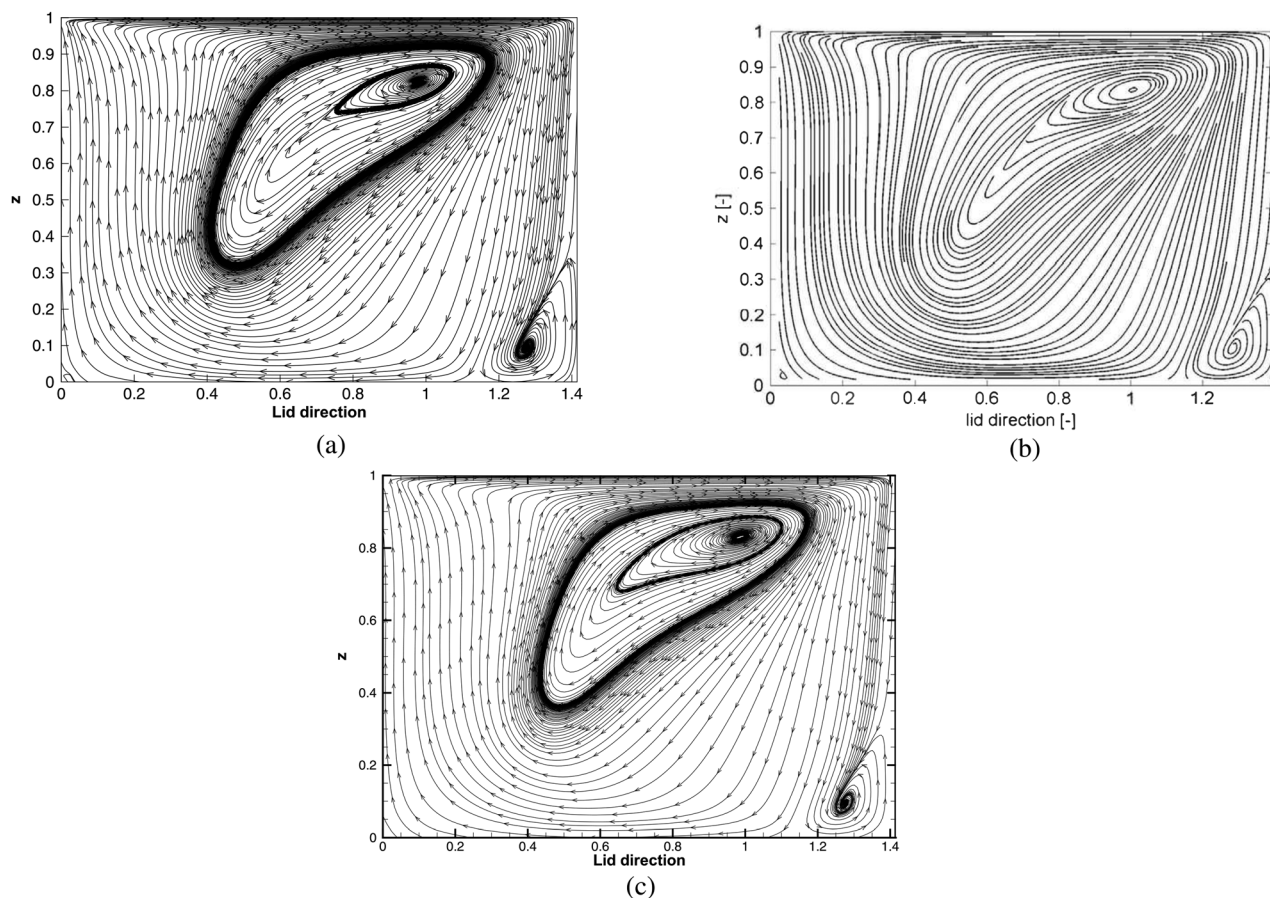


FIG. 16. Comparisons of the flow in the plane-parallel to the direction of the lid ( $y = x$ ) at  $Re = 700$  for (a) our results, (b) Asinari's results,<sup>36</sup> and (c) Yu's results.



$49 \times 49 \times 49$ , CPU time consumed using Scheme-P with BC1 may save the computational time by 58.7%, 57.6%, and 43.0% and for Reynolds number being 100, 400, and 700, respectively. With Reynolds number being 1000, CPU time consumed using the Yu-modified method<sup>5</sup> with grid sizes  $49 \times 49 \times 49$  and  $65 \times 65 \times 65$  is 2.70 times and 2.74 times using Scheme-P at  $49 \times 49 \times 49$  and  $65 \times 65 \times 65$ , respectively. Meanwhile, it is easily seen from Tables VIII and IX that with the increase in Reynolds number, Scheme-M takes a significant amount of computing CPU time compared to Scheme-P. Moreover, it is noticed that using the mesh size of  $65 \times 65 \times 65$ , Scheme-S with BC1 is not convergent when the Reynolds number  $Re$  achieves 2000, while at  $Re = 1000$ , although a convergent solution can be obtained by using Scheme-S, its error is obvious and the CPU time taken is 1.91 times that of Scheme-P with BC1. This means that for a larger Reynolds number, Scheme-P is comprehensively superior to Scheme-M and the Scheme-S in terms of

accuracy, convergence, and efficiency. Overall, for the diagonally lid-driven cavity flow problem, the newly proposed Scheme-P with BC1 achieves superior performance compared with Scheme-M, Scheme-S, and the Yu-modified method in terms of accuracy, convergence, and efficiency.

For further understanding the physical characteristics of the diagonally lid-driven cavity flow, some flow patterns obtained using Scheme-P with BC1 for this flow problem would be provided in the subsection. First of all, the 3D streamline from two views are displayed in Figs. 10–14 for different  $Re = 100, 400, 700, 1000$ , and 2000. This problem is reflection symmetric with respect to the diagonally plane being parallel to the driven direction, so the primary flow is shown at the main diagonally plane. For  $Re = 1000$ , the results reported by Feldman and Gelfgat<sup>8</sup> indicated that the flow pattern in this problem is fully three-dimensional and is characterized by one primary and one secondary downstream eddy whose centers are located on the

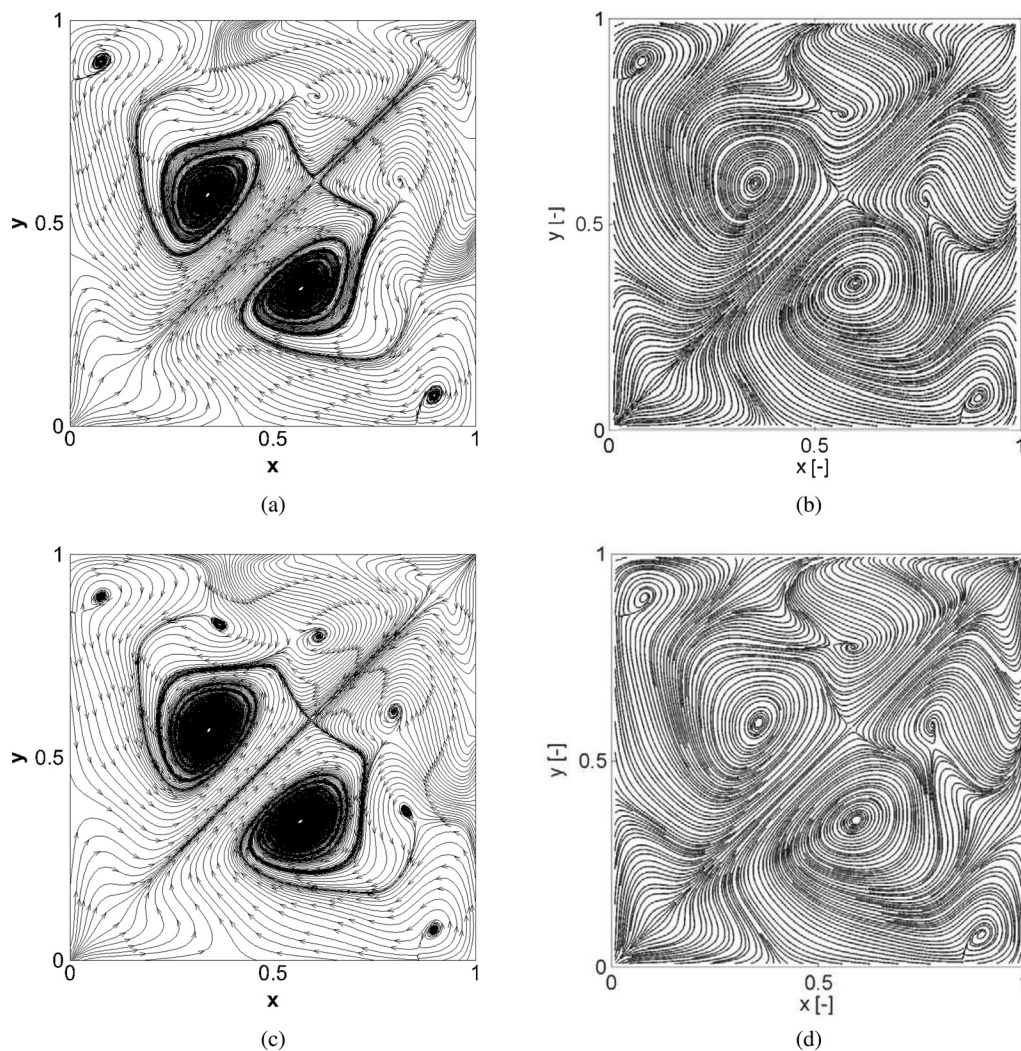


**FIG. 17.** Comparisons of the flow in the middle plane ( $z = 0.5$ ) at  $Re = 2000$  between our results with grid sizes (a)  $49^3$  and (c)  $65^3$  and Asinari's results<sup>36</sup> with grid sizes (b)  $49^3$  and (d)  $69^3$ .

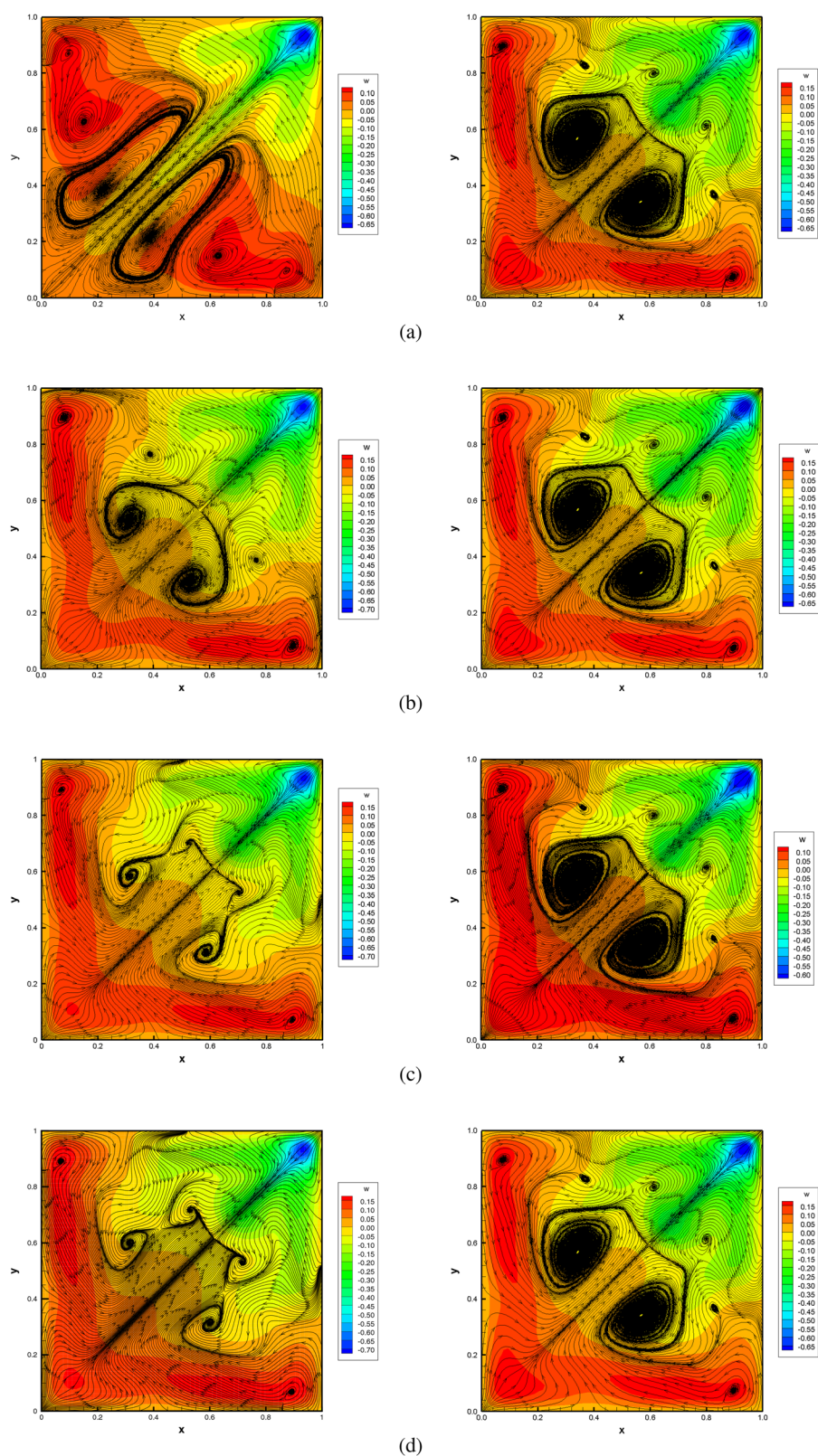


**FIG. 18.** Comparisons of the flow in the middle plane ( $z=0.5$ ) at  $Re=2000$  between Scheme-P's results (right) and Yu's results (left) with different convergence criteria: (a)  $10^{-7}$ ; (b)  $4 \times 10^{-8}$ , (c)  $4 \times 10^{-9}$ ; (d)  $10^{-9}$ .



symmetry plane. As seen from Figs. 10–14, the flow characteristics observed in Ref. 8 at  $Re = 1000$  are also observed for the Reynolds numbers ranging from 100 to 2000. There are one primary eddy and one secondary downstream eddies on the symmetry plane, but no evidence of the secondary upstream eddy observed in the standard lid-driven cavity, except the case  $Re = 2000$ . It can be found that the center of the primary eddy gradually moves toward the below left region of the symmetry plane as the Reynolds number increases. In addition, no any two-dimensional similarities are seen from this flow. Moreover, the flows for  $Re = 700$  in the plane perpendicular and parallel to the direction of the lid are exhibited in Figs. 15 and 16, respectively. As seen in Figs. 15 and 16, the flow structures obtained using Scheme-P with BC1 agree well with those solved by the link-wise artificial compressibility method in Ref. 36 and the fourth-order compact

method using the modified streamfunction formulation with BC1 in Ref. 5. In particular, it can be noticed from Fig. 17 that the results computed by Scheme-P for  $Re = 2000$  with grid sizes  $49 \times 49 \times 49$  and  $65 \times 65 \times 65$  are in good agreement with the result obtained in Ref. 36 using grid sizes  $49 \times 49 \times 49$  and  $69 \times 69 \times 69$ , respectively. However, it is clearly seen that the result calculated in Ref. 5 do not match the one given in Ref. 36. These are reflected from the data for  $Re = 2000$  in Table X. Furthermore, the diagonally lid-driven cavity flow at  $Re = 2000$  is also solved with different convergence criteria to verify the robustness of Scheme-P with BC1. Figure 18 provides four flow patterns in the middle plane  $z = 0.5$  at  $Re = 2000$  using the present Scheme-P with BC1 and the Yu-modified method<sup>5</sup> when the convergence criteria of  $10^{-7}$ ,  $4 \times 10^{-8}$ ,  $4 \times 10^{-9}$ , and  $10^{-9}$  are set. Notice from Fig. 18 that although both methods can obtain a convergent solution under the four

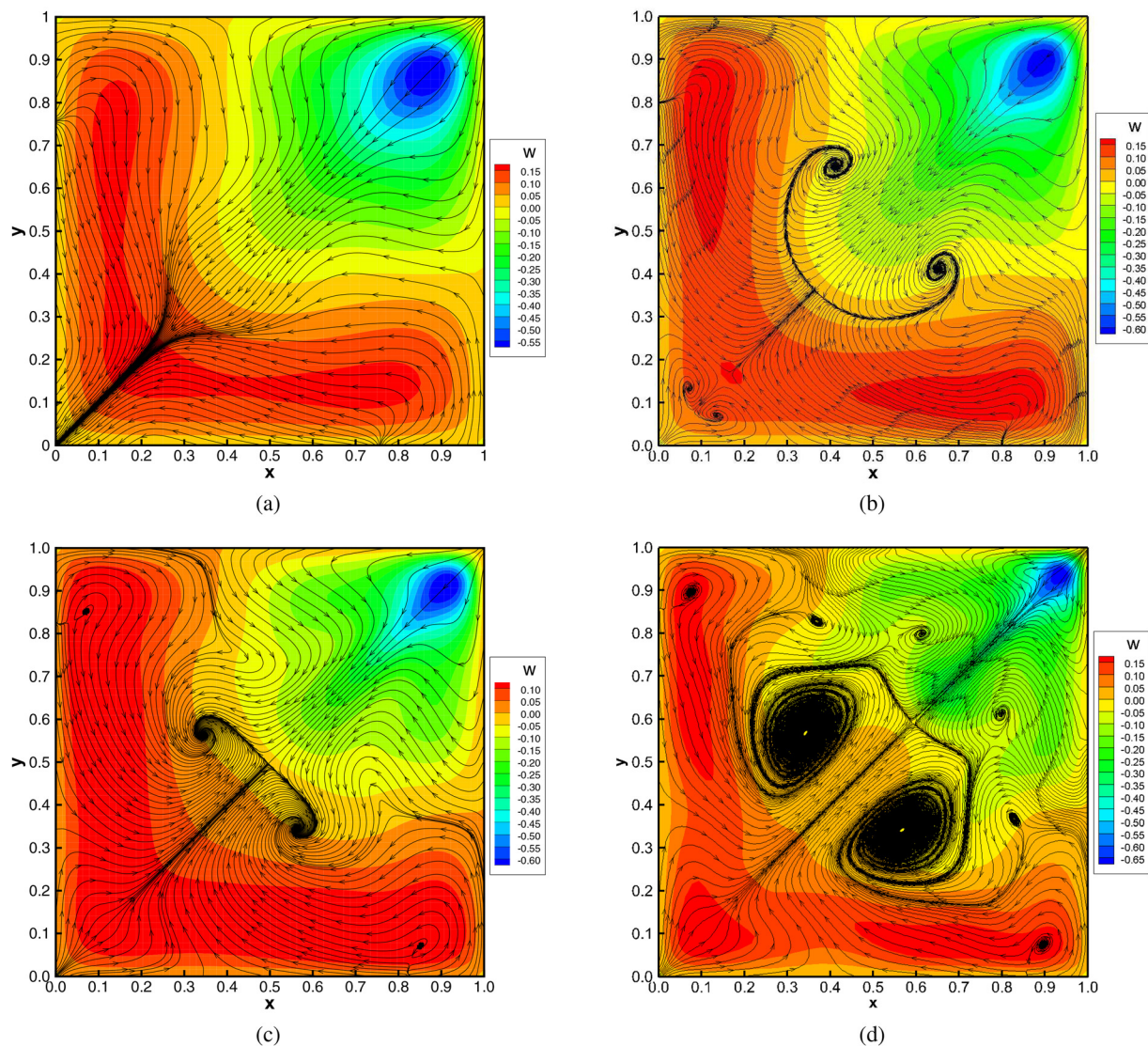


FIG. 19. Flow in the middle plane ( $z = 0.5$ ) for (a)  $Re = 400$ , (b)  $Re = 700$ , (c)  $Re = 1000$ , and (d)  $Re = 2000$ .

convergence criteria, the corresponding four flow patterns obtained by the Yu-modified method are significantly different from each other, and are not consistent with that given in Ref. 36 on the whole. On the contrary, the corresponding four flow patterns obtained by Scheme-P with BC1 are not only in good agreement with that obtained in Ref. 36 but are also almost indistinguishable, indicating that the Scheme-P with BC1 has a high-resolution and is robust and reliable.

Finally, Fig. 19 shows the flow patterns in the middle plane  $z = 0.5$  from  $Re = 400$  to  $Re = 2000$  using the present Scheme-P with BC1. With the increase in the Reynolds number, more pairs of vortex can be observed, which is very similar to previous findings.<sup>34,36,37</sup> Especially when  $Re = 2000$ , another vortex pair is also resolved using Scheme-P with BC1 compared with the existing results in the literature.

## VI. CONCLUSION

In this paper, a new fourth-order compact difference method has been developed for the 3D steady incompressible viscous flows in the cases of no in-flow and out-flow on the boundaries. The physics-preserving pure streamfunction formulation of 3D incompressible NS equations has been established based on the first-type boundary condition (BC1), which enforces divergence-free conditions and can ensure existence and uniqueness of solutions mathematically. Both of the streamfunction-vector components and their first-order partial derivatives are treated as unknown variables and are used to construct the fourth-order compact schemes for the pure streamfunction formulation. New high-order numerical boundary schemes have been proposed for the first-type boundary condition (BC1). To assess the performance of the proposed fourth-order compact schemes, three fluid flow problems have been solved numerically using Scheme-P, Scheme-M, and Scheme-S that are based on the physics-preserving formulation, the modified and the simplified pure streamfunction formulations with BC1, respectively. The obtained results using Scheme-P are in excellent agreement with available results in the literature, indicating that the present proposed method is accurate and effective. An only small singularity and a more singular problems show that the newly proposed Scheme-P with BC1 based on the physics-preserving pure streamfunction formulation can give precise convergent solutions and save computational cost and time, which is significantly superior to the method developed in Ref. 5. Therefore, it has the ability to accurately and efficiently simulate various 3D flows problems.

Finally, it should be noticed that to provide more details of flows such as the critical Reynolds numbers listed in Refs. 35, 44, 50, and 51, the unsteady incompressible NS equations should be solved. Thus, an extension of the present high-order compact approach to solve the unsteady incompressible NS equations in a 3D pure streamfunction formulation form is necessary and under way. Moreover, it is worth emphasizing that for incompressible 3D flows, the practitioners and CFD (Computational Fluid Dynamics) software packages typically use the SIMPLE-type algorithms,<sup>52,53</sup> the comparison of the present 3D streamfunction approach to SIMPLE-type algorithm in terms of efficiency is also a significant and valuable work. Another topic that may be of interest is the extension of the present method to non-rectangular geometric problem because the present compact scheme is confined to rectangular domain. Given that they are beyond the scope of the present study, these works will be carried out in the future.

## ACKNOWLEDGMENTS

We would like to thank the referees for their comments and suggestions. This work was supported by the National Natural Science Foundation of China under Grant Nos. 11872151, 91330112, and 11372075 and the Special Program for Applied Research on Super-Computation of the NSFC-Guangdong Joint Fund (the fourth phase).

## AUTHOR DECLARATIONS

### Conflict of Interest

The authors have no conflicts to disclose.

### Author Contributions

**Bo Peng:** Data curation (equal); Formal analysis (equal); Validation (equal); Visualization (equal); Writing – review & editing (equal). **Xiaohu Guo:** Conceptualization (supporting); Formal analysis (supporting); Writing – review & editing (equal). **Yingqing Zu:** Formal analysis (equal); Methodology (supporting); Writing – review & editing (supporting). **Zhenfu Tian:** Conceptualization (equal); Formal analysis (equal); Funding acquisition (equal); Methodology (equal); Writing – original draft (equal); Writing – review & editing (equal).

## DATA AVAILABILITY

The data that support the findings of this study are available within the article.

## APPENDIX: HIGH-ORDER COMPACT SCHEMES FOR THE FIRST-ORDER PARTIAL DERIVATIVES

In this appendix, the fourth- and the sixth-order Padé compact difference schemes given in the literature<sup>38</sup> for the first-order partial derivative are provided to obtain the fourth-order compact schemes for higher-order partial derivatives and Eq. (3) in this paper.

### 1. Fourth-order compact difference schemes

For all of the first-order partial derivatives at the interior points including the face inner points in the text, the fourth-order Padé compact difference scheme used is as follows:

$$\left(1 + \frac{h_x^2}{6}\delta_x^2\right)F_{i,x} = \delta_x\psi_i, \quad i = 1, 2, 3, \quad (\text{A1})$$

where  $F_{i,x}$  is the approximation for the first-order partial derivatives of  $\psi_i$  ( $i = 1, 2, 3$ ),  $h_x$  is the spatial grid size, and  $\delta_x$  and  $\delta_x^2$  are the standard three-point second-order central difference operators defined in Eq. (11).

Scheme (A1) was proposed in Ref. 18 and can be rewritten as

$$F_{i,xm-1} + 4F_{i,xm} + F_{i,xm+1} = \frac{3}{h_x}(\psi_{im+1} - \psi_{im-1}), \quad (\text{A2})$$

where  $1 \leq m \leq N_x - 1$ ,  $i = 1, 2, 3$ .

Using the Taylor series expansion, the truncation error of Eq. (A1) is obtained by



$$F_{i,\alpha} = \frac{\partial \psi_i}{\partial \alpha} - \frac{h_x^4}{180} \frac{\partial^5 \psi_i}{\partial \alpha^5} + O(h_x^6), \quad i = 1, 2, 3, \quad (\text{A3})$$

which shows that the scheme (A1) or (A2) is of fourth-order accuracy.

Scheme (A2) subject to the known or determined boundary conditions of the  $\frac{\partial \psi_i}{\partial \alpha}$  ( $i = 1, 2, 3$ ) can be directly solved. Unfortunately, the  $\frac{\partial \psi_i}{\partial \alpha}$  ( $i = 1, 2, 3$ ) at the boundary is not always known or can be determined by known conditions. For example, on the whole face  $z = 1$ , the partial derivatives  $\frac{\partial \psi_3}{\partial x}$  and  $\frac{\partial \psi_3}{\partial y}$  are unknown. Thus, in order to obtain  $\frac{\partial \psi_3}{\partial x}$  and  $\frac{\partial \psi_3}{\partial y}$  for the face interior points at  $z = 1$  by means of Eq. (A2), we have to supplement numerical boundary schemes for  $\frac{\partial \psi_3}{\partial x}$  and  $\frac{\partial \psi_3}{\partial y}$ . Therefore, the following boundary closures are suggested:

$$\begin{aligned} F_{i,\alpha 0} + 3F_{i,\alpha 1} &= \frac{1}{6h_x} (-17\psi_{i0} + 9\psi_{i1} + 9\psi_{i2} - \psi_{i3}), \\ 3F_{i,\alpha N_x-1} + F_{i,\alpha N_x} &= \frac{1}{6h_x} (\psi_{iN_x-3} - 9\psi_{iN_x-2} \\ &\quad - 9\psi_{iN_x-1} + 17\psi_{iN_x-3}), \end{aligned} \quad (\text{A4})$$

in which  $i = 1, 2, 3$ . The schemes (A4) are of fourth-order ones<sup>5</sup> and can be found in Ref. 53.

## 2. Sixth-order compact difference schemes

To establish the fourth-order compact scheme for the pure streamfunction formulation in this paper, in addition to providing the fourth-order compact schemes, one also needs to provide higher-order accuracy schemes for the first-order partial derivatives  $\frac{\partial \psi_i}{\partial \alpha}$  ( $i = 1, 2, 3$ ).

For the interior mesh points ( $2 \leq m \leq N_x - 2$ ), according to Ref. 38, the sixth-order Padé schemes for the first-order partial derivatives  $\frac{\partial \psi_i}{\partial \alpha}$  ( $i = 1, 2, 3$ ) are provided as follows:

$$\frac{1}{3} \bar{F}_{i,\alpha m-1} + \bar{F}_{i,\alpha m} + \frac{1}{3} \bar{F}_{i,\alpha m+1} = \frac{14}{9} \frac{\psi_{im+1} - \psi_{im-1}}{2h_x} + \frac{1}{9} \frac{\psi_{im+2} - \psi_{im-2}}{4h_x}, \quad (\text{A5})$$

where  $\bar{F}_{i,\alpha}$  are higher-order accurate approximations of the first-order partial derivatives  $\frac{\partial \psi_i}{\partial \alpha}$  ( $i = 1, 2, 3$ ).

Using the Taylor series expansion, the truncation errors of Eq. (A5) is obtained by

$$F_{i,\alpha} = \frac{\partial \psi_i}{\partial \alpha} + \frac{h_x^6}{2100} \frac{\partial^7 \psi_i}{\partial \alpha^7} + O(h_x^8), \quad l = 1, 2, 3, \quad (\text{A6})$$

which shows that the scheme (A5) is of the sixth-order accuracy.

At near-boundary points, the following one-sided approximations with fifth-order accuracy are utilized for  $\frac{\partial \psi_i}{\partial \alpha}$  ( $i = 1, 2, 3$ )

$$\begin{aligned} \frac{1}{10} \bar{F}_{i,\alpha 0} + \frac{6}{10} \bar{F}_{i,\alpha 1} + \frac{3}{10} \bar{F}_{i,\alpha 2} \\ = -\frac{10\psi_{i0} + 9\psi_{i1} - 18\psi_{i2} - \psi_{i3}}{30h_x} \\ \frac{3}{10} \bar{F}_{i,\alpha N_x-2} + \frac{6}{10} \bar{F}_{i,\alpha N_x-1} + \frac{1}{10} \bar{F}_{i,\alpha N_x} \\ = -\frac{\psi_{iN_x-3} + 18\psi_{iN_x-2} - 9\psi_{iN_x-1} - 10\psi_{iN_x}}{30h_x}. \end{aligned} \quad (\text{A7})$$

Considering the fact that the boundary values of  $\frac{\partial \psi_i}{\partial \alpha}$  are either known or have been determined, the approximate derivatives  $\bar{F}_{i,\alpha}$  with higher-order accuracy would be obtained by taking advantage of the Padé relation (A5) combining with (A7).

The approximations (A5) and (A7) can be found in Ref. 53. In addition, they have been used in Refs. 2 and 20 for constructing fourth-order accurate approximations for 2D and 3D pure streamfunction formulation of the incompressible NS equations successfully.

## REFERENCES

- V. Ruas and L. Quartapelle, "Uncoupled finite element solution of biharmonic problems for vector potentials," *Int. J. Numer. Methods Fluids* **11**, 811–822 (1990).
- D. Fishelov, M. Ben-Artzi, and J. P. Croisille, "Recent developments in the pure streamfunction formulation of the Navier-Stokes system," *J. Sci. Comput.* **45**, 238–258 (2010).
- M. Ben-Artzi, J. P. Croisille, D. Fishelov, and S. Trachtenberg, "A pure-compact scheme for the streamfunction formulation of Navier-Stokes equations," *J. Comput. Phys.* **205**, 640–664 (2005).
- S. Sen, "A new family of (5,5)CC-4OC schemes applicable for unsteady Navier-Stokes equations," *J. Comput. Phys.* **251**, 251–271 (2013).
- P. X. Yu and Z. F. Tian, "A high-order compact scheme for the pure streamfunction (vector potential) formulation of the 3D steady incompressible Navier-Stokes equations," *J. Comput. Phys.* **382**, 65–85 (2019).
- E. Weinan and J. Liu, "Finite difference methods for 3D viscous incompressible flows in the vorticity-vector potential formulation on nonstaggered grids," *J. Comput. Phys.* **138**, 57–82 (1997).
- C. Shu, L. Wang, and Y. T. Chew, "Numerical computation of three-dimensional incompressible Navier-Stokes equations in primitive variable form by DQ method," *Int. J. Numer. Methods Fluids* **43**, 345–368 (2003).
- Y. Feldman and A. Y. Gelfgat, "From multi- to single-grid CFD on massively parallel computers: Numerical experiments on lid-driven flow in a cube using pressure-velocity coupled formulation," *Comput. Fluids* **46**, 218–223 (2011).
- S. Albensoeder and H. C. Kuhlmann, "Accurate three-dimensional lid-driven cavity flow," *J. Comput. Phys.* **206**, 536–558 (2005).
- Y. N. He and W. W. Sun, "Stability and convergence of the Crank-Nicolson/Adams-Bashforth scheme for the time-dependent Navier-Stokes equations," *SIAM J. Numer. Anal.* **45**, 837–869 (2007).
- J. Chen, P. Yu, Z. F. Tian, and H. Ouyang, "A high-order compact scheme for solving the 2D steady incompressible Navier-Stokes equations in general curvilinear coordinates," *Int. J. Numer. Methods Fluids* **92**, 456–477 (2020).
- S. Albensoeder, H. C. Kuhlmann, and H. J. Rath, "Three-dimensional centrifugal-flow instabilities in the lid-driven-cavity problem," *Phys. Fluids* **13**, 121–135 (2001).
- V. S. Yadav, V. Maurya, P. K. Maurya, and M. K. Rajpoot, "Novel hybrid compact schemes for stream function-velocity formulation of the incompressible Navier-Stokes equations," *Phys. Fluids* **35**, 017114 (2023).
- N. Sharma and T. K. Sengupta, "Vorticity dynamics of the three-dimensional Taylor-Green vortex problem," *Phys. Fluids* **31**, 035106 (2019).
- N. Sharma, T. K. Sengupta, and J. R. Brinkerhoff, "Non-linear instability analysis of the three-dimensional Navier-Stokes equations: Taylor-Green vortex problem," *Phys. Fluids* **32**, 064102 (2020).
- P. J. Roache, *Computational Fluid Dynamics* (Hermosa Press, Albuquerque, NM, 1972).
- S. V. Patankar and D. B. Spalding, "A calculation procedure for heat, mass and momentum transfer in three-dimensional parabolic flows," *Int. J. Heat Mass Transfer* **15**, 1787–1806 (1972).
- R. S. Hirsh, "Higher order accurate difference solutions of fluid mechanics problems by a compact differencing technique," *J. Comput. Phys.* **19**, 90–109 (1975).
- K. L. Wong and A. J. Baker, "A 3D incompressible Navier-Stokes velocity-vorticity weak form finite element algorithm," *Int. J. Numer. Methods Fluids* **38**, 99–123 (2002).

- <sup>20</sup>M. Ben-Artzi, J. P. Croisille, and D. Fishelov, "A high order compact scheme for the pure-streamfunction formulation of the Navier-Stokes equations," *J. Sci. Comput.* **42**, 216–250 (2010).
- <sup>21</sup>D. Fishelov, "A new fourth-order compact scheme for the Navier-Stokes equations in irregular domains," *Comput. Math. Appl.* **74**, 6–25 (2017).
- <sup>22</sup>M. Ben-Artzi, D. Fishelov, and S. Trachtenberg, "Vorticity dynamics and numerical resolution of Navier-Stokes equations," *Math. Model. Numer. Anal.* **35**, 313–330 (2001).
- <sup>23</sup>Z. F. Tian and P. X. Yu, "An efficient compact difference scheme for solving the streamfunction formulation of the incompressible Navier-Stokes equations," *J. Comput. Phys.* **230**, 6404–6419 (2011).
- <sup>24</sup>P. X. Yu and Z. F. Tian, "Compact computations based on a streamfunction-velocity formulation of two-dimensional steady laminar natural convection in a square cavity," *Phys. Rev. E* **85**, 036703 (2012).
- <sup>25</sup>P. X. Yu, J. X. Qiu, Q. Qin, and Z. F. Tian, "Numerical investigation of natural convection in a rectangular cavity under different directions of uniform magnetic field," *Int. J. Heat Mass Transfer* **67**, 1131–1144 (2013).
- <sup>26</sup>P. X. Yu, Z. F. Tian, A. Y. Ying, and M. A. Abdou, "Stream function-velocity-magnetic induction compact difference method for the 2D steady incompressible full magnetohydrodynamic equations," *Comput. Phys. Commun.* **219**, 45–69 (2017).
- <sup>27</sup>M. M. Gupta and J. C. Kalita, "A new paradigm for solving Navier-Stokes equations: Streamfunction-velocity formulation," *J. Comput. Phys.* **207**, 52–68 (2005).
- <sup>28</sup>J. X. Qiu, B. Peng, and Z. F. Tian, "A compact streamfunction-velocity scheme for the 2-D unsteady incompressible Navier-Stokes equations in arbitrary curvilinear coordinates," *J. Hydrodyn.* **31**, 827–839 (2019).
- <sup>29</sup>A. Rubel and G. Volpe, "Biharmonic vector stream function formulation and multigrid solution for a three-dimensional driven-cavity Stokes flow," AIAA Paper No. 1989-1968, 1989.
- <sup>30</sup>D. L. Young, C. H. Tsai, and C. S. Wu, "A novel vector potential formulation of 3D Navier-Stokes equations with through-flow boundaries by a local meshless method," *J. Comput. Phys.* **300**, 219–240 (2015).
- <sup>31</sup>A. M. Elshabka and T. J. Chung, "Numerical solution of three-dimensional stream function vector components of vorticity transport equations," *Comput. Methods Appl. Mech. Eng.* **170**, 131–153 (1999).
- <sup>32</sup>A. Povitsky, "Three-dimensional flow with elevated helicity in driven cavity by parallel walls moving in perpendicular directions," *Phys. Fluids* **29**, 083601 (2017).
- <sup>33</sup>A. Povitsky, "Mixing in three-dimensional cavity by moving cavity walls," *Theor. Comput. Fluid Dyn.* **34**, 593–617 (2020).
- <sup>34</sup>A. Povitsky, "High-incidence 3-D lid-driven cavity flow," AIAA Paper No. 01-2847, 2001.
- <sup>35</sup>Y. Feldman, "Theoretical analysis of three-dimensional bifurcated flow inside a diagonally lid-driven cavity," *Theor. Comput. Fluid Dyn.* **29**, 245–261 (2015).
- <sup>36</sup>P. Asinari, T. Ohwada, E. Chiavazzo, and A. F. Di Rienzo, "Link-wise artificial compressibility method," *J. Comput. Phys.* **231**, 5109–5143 (2012).
- <sup>37</sup>J. Wang and D. Wan, "Parallel simulation of 3D lid-driven cubic cavity flows at yaw by finite element method," *Ocean Eng.* **33**, 1–12 (2015) (in Chinese).
- <sup>38</sup>S. K. Lele, "Compact finite difference schemes with spectral-like resolution," *J. Comput. Phys.* **103**, 16–42 (1992).
- <sup>39</sup>Z. J. Wang, K. Fidkowski, R. Abgrall, F. Bassi, D. Caraeni, A. Cary, H. Deconinck, R. Hartmann, K. Hillewaert, H. T. Huynh, N. Kroll, G. May, P.-O. Persson, B. van Leer, and M. Visbal, "High-order CFD methods: Current status and perspective," *Int. J. Numer. Methods Fluids* **72**, 811–845 (2013).
- <sup>40</sup>L. Caban and A. Tyliczszak, "High-order compact difference schemes on wide computational stencils with a spectral-like accuracy," *Comput. Math. Appl.* **108**, 123–140 (2022).
- <sup>41</sup>Z. F. Tian, "Research on high accuracy compact finite difference methods and their applications," Ph.D. thesis (Shanghai University, China, 2006) (in Chinese).
- <sup>42</sup>J. W. Stephenson, "Single cell discretizations of order two and four for biharmonic problems," *J. Comput. Phys.* **55**, 65–80 (1984).
- <sup>43</sup>J. K. Kim and D. J. Lee, "Optimized compact finite difference schemes with maximum resolution," *AIAA J.* **34**, 887–893 (1996).
- <sup>44</sup>J. K. Zhang, M. Cui, Z. L. Zuo, S. Y. Luo, J. X. Guo, and Z. Z. Qiu, "Prediction on steady-oscillatory transition via Hopf bifurcation in a three-dimensional (3D) lid-driven cube," *Comput. Fluids* **229**, 105068 (2021).
- <sup>45</sup>Y. Feldman and A. Y. Gelfgat, "Oscillatory instability of a three-dimensional lid-driven flow in a cube," *Phys. Fluids* **22**, 093602 (2010).
- <sup>46</sup>B. N. Jiang, T. L. Lin, and L. A. Povinelli, "Large-scale computation of incompressible viscous flow by least-squares finite element method," *Comput. Methods Appl. Mech. Eng.* **14**, 213–231 (1994).
- <sup>47</sup>D. C. Lo, K. Murugesan, and D. L. Young, "Numerical solution of three-dimensional velocity-vorticity Navier-Stokes equations by finite difference method," *Int. J. Numer. Methods Fluids* **47**, 1469–1487 (2005).
- <sup>48</sup>D. d'Humières, I. Ginzburg, M. Krafczyk, M. Lallemand, and L.-S. Luo, "Multiple-relaxation-time lattice Boltzmann models in three dimensions," *Philos. Trans. R. Soc. London, Ser. A* **360**, 437–451 (2002).
- <sup>49</sup>V. E. Sonzogni, A. M. Yommi, N. M. Nigro, and M. A. Storti, "A parallel finite element program on a Beowulf cluster," *Adv. Eng. Software* **33**, 427–443 (2002).
- <sup>50</sup>A. Y. Gelfgat, "Linear instability of the lid-driven flow in a cubic cavity," *Theor. Comput. Fluid Dyn.* **33**, 59–82 (2019).
- <sup>51</sup>H. C. Kuhlmann and S. Albensoeder, "Stability of the steady three-dimensional lid-driven flow in a cube and the supercritical flow dynamics," *Phys. Fluids* **26**, 024104 (2014).
- <sup>52</sup>S. V. Patankar, *Numerical Heat Transfer and Fluid Flow* (Hemisphere Publishing, Washington D.C., 1980).
- <sup>53</sup>M. H. Carpenter, D. Gottlieb, and S. Abarbanel, "The stability of numerical boundary treatments for compact high-order schemes finite difference schemes," *J. Comput. Phys.* **108**, 272–295 (1993).